



HAL
open science

Estimating sediment transport diffusion coefficients from reconstructed rifted margin architecture: measurements in the Ogooué and Zambezi deltas

Brendan Simon, Cécile Robin, Delphine Rouby, Jean Braun, François Guillocheau

► To cite this version:

Brendan Simon, Cécile Robin, Delphine Rouby, Jean Braun, François Guillocheau. Estimating sediment transport diffusion coefficients from reconstructed rifted margin architecture: measurements in the Ogooué and Zambezi deltas. *Basin Research*, 2022, 10.1111/bre.12696 . insu-03736460

HAL Id: insu-03736460

<https://insu.hal.science/insu-03736460>

Submitted on 22 Jul 2022

HAL is a multi-disciplinary open access archive for the deposit and dissemination of scientific research documents, whether they are published or not. The documents may come from teaching and research institutions in France or abroad, or from public or private research centers.

L'archive ouverte pluridisciplinaire **HAL**, est destinée au dépôt et à la diffusion de documents scientifiques de niveau recherche, publiés ou non, émanant des établissements d'enseignement et de recherche français ou étrangers, des laboratoires publics ou privés.

Estimating sediment transport diffusion coefficients from reconstructed rifted margin architecture: measurements in the Ogooué and Zambezi deltas

Brendan SIMON^{(1)#}

⁽¹⁾ Géosciences Environnement Toulouse – UMR 5563, 14 av. Edouard Belin, 31400 Toulouse, France.

corresponding author: brendan.simon@outlook.fr

ORCID: <https://orcid.org/0000-0002-2753-5158>

Cécile Robin⁽²⁾

⁽²⁾ CNRS, Géosciences Rennes, UMR 6118, Université de Rennes 1, Rennes, 35042, France.

cecile.robin@univ-rennes1.fr

ORCID: <https://orcid.org/0000-0002-7394-4438>

Delphine ROUBY^{(1)#}

⁽¹⁾ Géosciences Environnement Toulouse – UMR 5563, 14 av. Edouard Belin, 31400 Toulouse, France.

corresponding author: delphine.Rouby@get.omp.eu

ORCID : <https://orcid.org/0000-0003-2827-0566>

Jean BRAUN⁽³⁾

⁽³⁾ GFZ German Research Centre for Geosciences – Heinrich-Mann-Allee 18/19, Building HMA 18/19, 14473 Potsdam, Germany

jbraun@gfz-potsdam.de

ORCID:

François GUILLOCHEAU⁽²⁾

⁽²⁾ CNRS, Géosciences Rennes, UMR 6118, Université de Rennes 1, Rennes, 35042, France.

francois.guillocheau@univ-rennes1.fr

ORCID : <https://orcid.org/0000-0002-8299-439X>

Funding statement/information

This study was realized in the frame of the COLORS (Coupling Lithosphere Deformation and Stratigraphy) project funded by TotalEnergies.

Data Availability Statement

The seismic and well data supporting this study were made available by TotalEnergies. The authors are not allowed to share the data, which were used under license for this study.

The authors declare no conflict of interest.

This article has been accepted for publication and undergone full peer review but has not been through the copyediting, typesetting, pagination and proofreading process which may lead to differences between this version and the [Version of Record](#). Please cite this article as doi: [10.1111/bre.12696](https://doi.org/10.1111/bre.12696)

ACKNOWLEDGMENTS

This work is part of the COLORS (Coupling Lithosphere Deformation and Stratigraphy) project funded by TotalEnergies. We thank Massimo Dall'asta, Charlotte Fillon, Laure Guerit and Xiaoping Yuan for the helpful discussions. We thank Neil Mitchell, John Armitage and editor Peter Burgess for their comments which significantly improved this paper.

ABSTRACT

Diffusion-based stratigraphic models are widely used to simulate sedimentary systems and margin deltas. Diffusion-based models assume that the topographic evolution primarily depends from its slope. Limited attention has however been given to the calibration of the transport coefficients. Here, we evaluate transport coefficient values from natural examples, the Ogooué and Zambezi rifted margin deltas over the last 5 to 12 Ma respectively. We developed a method to estimate transport coefficients based on high resolution seismic stratigraphy analysis of the stratigraphic architecture of these deltas. For each stratigraphic sequence, we calibrated the sand/shale ratios of the deposits, we restored their depositional slopes, we estimated their uncompacted accumulated volumes and we calculated the transport coefficient (K_d) from the sediment flux / slope ratio.

Estimated values of K_d fall within one order of magnitude ($\times 0.1 \text{ km}^2/\text{ka}$), a much narrower range than previously published values ($\times 0.0001$ to $\times 100 \text{ km}^2/\text{ka}$). We show that the diffusion approximation is optimal at 10 - 100 km scale and 0.5 - 1 Ma time resolution, independently of the stratigraphic context. We show that the diffusion assumption is appropriate for the formation of the clinoforms (mainly gravity driven). It is however not optimal for the shelf and distal domains where additional processes (e.g. wave, flood, hemipelagic, turbidites, oceanic current), not accounted for in the diffusion assumption, significantly impact sediment transport. We documented a significant increase of K_d values after 0.9 Ma, coeval of an increase in the amplitude of eustatic variations at this time indicating that the calibration of K_d from present day sedimentary systems might not be optimal for simulations of sedimentary systems before the last million years.

KEYWORDS

Rifted margin, stratigraphic numerical model, diffusion coefficient calibration, sequence-stratigraphy, Ogooué Delta, Zambezi Delta.

INTRODUCTION

Since the early work of Culling (1960) and Carson and Kirkby (1972), diffusion-based models used to simulate landscape evolution have been extended to the marine environment to reproduce progradation of deltas (Kenyon and Turcotte, 1985) and continental shelves (Jordan and Flemings, 1991; Kaufman et al., 1991; Rivenaes, 1992, 1997; Granjeon, 1996; Granjeon and Joseph, 1999; Mitchell and Huthnance, 2008). Diffusion-based models for the marine environment relies on the assumption that transport is driven by gravity and is proportional to the topographic gradient following a diffusion (or transport) coefficient K_d (i.e., transport efficiency for a given grain size). This simple formulation is widely used to investigate interplay between the main factors controlling stratigraphic architectures (e.g., eustasy, subsidence, sediment supply; e.g., Reynolds et al., 1991; Posamentier and Allen, 1993; Steckler et al., 1993; Carvajal and Steel, 2009; Burgess et al., 2012; Csato et al., 2014; Granjeon, 2014; Harris et al., 2015, 2016; Ding et al., 2019; Yuan et al., 2019).

Published values of diffusion coefficients have often been estimated from the present-day slopes and sedimentary fluxes in sedimentary systems based on a trial and error “best-fit” approach (Paola, 2000). As a consequence, the range of published values is very wide (Fig. 1; e.g., Syvitski et al., 1988; Flemings and Jordan, 1989; Jordan and Flemings, 1991; Kaufman et al., 1991; Rivenaes, 1992; Syvitski and Daughney, 1992; Burgess et al., 2006; Rohais et al., 2007; Csato et al., 2007, 2012, 2014; Clark et al., 2009; Leroux, 2012; Rouby et al., 2013; Leroux et al., 2014; Burgess and Prince, 2015; Yuan et al., 2019; Ding et al., 2019). Nevertheless, the implications of this range in terms of sedimentary processes in natural systems have not been fully investigated.

The aim of this work is first to provide values for the diffusion coefficient consistent with natural systems and not limited to the present-day climatic and geodynamic context. Second, it is also to evaluate the relevance of the diffusion assumption for approximating sediment transports in the context of rifted margin deltas. To do this, we developed an original method to estimate this coefficient from the stratigraphic architecture of natural examples, in particular, the ratios of the associated accumulation rates and slopes. We applied this method to two rifted margin shelf-edge deltas: the Plio-Pleistocene (5 - 0 Ma) of the Ogooué Delta in Gabon and the Mio-Pleistocene (12 - 0 Ma) of the Zambezi delta in Mozambique. We analyzed the variability of the accumulation rates, slopes and diffusion coefficients in relation to the temporal and spatial resolutions, the location along the depositional profile, the stratigraphic context and the geological time.

BACKGROUND TO STRATIGRAPHIC NUMERICAL MODELLING

Accepted Article

Paola (2000), Tetzlaff and Priddy (2001) and Overeem et al. (2005) grouped stratigraphic models into geometrical or dynamic classes depending on the type of laws used to approximate erosion, transport and deposition processes. Geometrical models simulate the consequences of sedimentary processes rather than the processes themselves (Overeem et al., 2005), that is to say, they simulate the result of erosion and sedimentation in response to changing environmental parameters (e.g., Strobel et al., 1989; Kendall et al., 1991; Thorne and Swift, 1991; Bowman and Vail, 1993; Wehr, 1993; Ross et al., 1994; Cross and Lessenger, 1999; Houston et al., 2000). To the contrary, dynamic models simulate sediment production, transport and deposition processes themselves and include diffusion-based models. They produce realistic-looking stratal patterns at the scale of the continental margin, that is to say ranging from fluvio-deltaic to slope-basin depositional environments.

Diffusion-based stratigraphic models rely on a small set of simple equations governing the long-term evolution of the continental margin stratigraphy without attempting to simulate individual transport events. Since the early work of Culling (1960) and Carson and Kirkby (1972), diffusion models have been used in various forms to simulate sediment transport. Numerous studies have shown that the transport in alluvial fans, rivers and floodplains (Begin et al., 1981; Murray and Paola, 1994; Parker et al., 1998; Coulthard et al., 2000) in mountains and foreland basins (Jordan and Flemings, 1991; Tucker and Slingerland, 1994) seems to obey the assumptions of the diffusion model. The diffusion assumption has been extended to simulate progradation of deltas (Kenyon and Turcotte, 1985) and continental shelves in marine environments (Jordan and Flemings, 1991; Kaufman et al., 1991; Rivenaes, 1992, 1997; Granjeon, 1996; Granjeon and Joseph, 1999; Mitchell and Huthnance, 2008). Transport along the depositional profile of a single grain-size is assumed to be gravity-driven and proportional to its gradient following a diffusion coefficient K_d (i.e., transport efficiency of the considered grain size) following:

$$Q_d = -K_d \frac{\partial h}{\partial x} = K_d \times S \quad (1)$$

with Q_d the flux of sediment (in m^2/s), K_d the diffusion coefficient (in m^2/s), $-\partial h/\partial x$ the gradient of the depositional profile and $S = -\partial h/\partial x$ the slope. We here use the positive term slope S to describe the stratigraphic geometries.

Three-dimensional diffusion-based stratigraphic models include DIBAFILL (Quiquerez et al., 2000), DIONISOS (Diffusive Oriented Normal and Inverse-Simulation Of Sedimentation; Granjeon, 1996; Granjeon and Joseph, 1999), pyBadlands (Salles and Hardiman, 2016; Salles, 2018; Salles et al., 2018;) and Fastscope (Braun and Willett, 2013; Yuan et al., 2019). DIBAFILL has mainly been used for generic experiments (Quiquerez et al., 2000), whereas DIONISOS has been used to reproduce natural systems (e.g., Euzen et al., 2004; Csato et

al., 2012; Leroux et al., 2014; Hawie et al., 2015; Kolodka et al., 2016; Candido et al., 2019). As a difference, pyBadlands and Fastscope simulate dynamically-linked sediment production, transport and deposition in a source-to-sink context allowing to simulate self-consistent sediment supply to the sedimentary basins. Diffusion-based stratigraphic models are widely used to investigate the interplay between the main factors controlling stratigraphic sequences (e.g., eustasy, tectonics, flexural isostasy, sediment supply, sediment compaction, basin physiography; e.g., Reynolds et al., 1991; Posamentier and Allen, 1993; Steckler et al., 1993; Burgess et al., 2006, 2012; Carvajal and Steel, 2009; Csato et al., 2014; Granjeon, 2014; Harris et al., 2015, 2016; Ding et al., 2019; Yuan et al., 2019). However, despite the wide use of diffusion-based models, the calibration of the values of the diffusion parameters from geological data remains under-investigated.

METHODOLOGY

To estimate diffusion (or transport) coefficients from the geometry of natural sedimentary systems, we developed a method using subsurface data (well logs, biostratigraphic constraints and 2D seismic reflection lines). From those, we defined the high-resolution stratigraphic architecture of the sedimentary system to defined stratigraphic sequences, age models for calibrating stratigraphic sequences in absolute ages as well as grain size distributions (sand/clay ratio) of the deposits along the depositional profile. For each stratigraphic sequence, we then estimated the slopes of sedimentary surfaces at time of deposition and the associated sediment accumulation (or deposition) rates. Diffusion coefficients were then calculated from the linear regression coefficient of the accumulation rate/slope ratio.

Basin analysis: seismic stratigraphy and age model

To establish the stratigraphic architecture of the sedimentary system, we used two complementary methods of seismic stratigraphy based on the characterization of (1) the seismic facies and stratal termination patterns (Mitchum et al., 1977) and (2) the offlap-break (shoreline or shelf-edge break) migration trough time (Helland-Hansen and Gjelberg, 1994; Helland-Hansen and Hampson, 2009; Helland-Hansen and Martinsen, 1996). We defined depositional sequences (Vail et al., 1977) bounded by key surfaces (SB= Sequence Boundary; MFS= Maximum Flooding Surface; MRS= Maximum Regressive Surface; Catuneanu et al., 2009), resulting from changes in the balance between accommodation space and sedimentary flux. These sequences record a seaward and landward migration of the shoreline through time, i.e., a progradation (regression) and a retrogradation (transgression). The regression is recorded by three main stratal units: (1) the Highstand Normal Regressive deposits (HNR) during the onset of the regression; (2) the Forced Regressive deposits (FR) contemporaneous of an aerial erosion onshore and (3) the Lowstand Normal Regressive deposits (LNR) at the end of the regression. The transgression is recorded by the transgressive deposits (T;

Catuneanu et al., 2009).

We used two ages models to calibrate key stratigraphic surface (MRS, MFS and SB) in absolute ages. The low-resolution age model calibrated used biostratigraphy (i.e., foraminifers or nannofossils biozones) available at wells. The high-resolution age model then further refined the calibration within these time intervals using known eustatic, climatic and orbital events when available. From these two calibrations, we evaluated the influence of two temporal resolution on our results.

Estimation of slopes and sediment flux

Clinoforms

We focused our calibrations on shelf-edge clinoforms units which are basinward-dipping accretionary surfaces building up at the transition between the proximal (shelf) and the distal domain (basin floor). These are key sedimentary systems or units widely used to study sediment transit within these two domains (Larue and Martinez, 1989; Thorne, 1995; Pirmez et al., 1998; Steel and Olsen, 2002; Henriksen et al., 2009, 2011; Patruno and Helland-Hansen, 2018). They are typically tens to hundreds of meters thick and represent time intervals of hundreds of thousands to several million years. They are also commonly used as paleogeography and paleobathymetry indicators (e.g., Rich, 1951; Mitchum et al., 1977; Pirmez et al., 1998; Steel and Olsen, 2002; Bullimore et al., 2005; Johannessen and Steel, 2005; Helland-Hansen and Hampson, 2009; Olariu and Steel, 2009; Glørstad-Clark et al., 2010; Patruno et al., 2015).

As the geometry of the clinoforms is modified by post-depositional processes (differential compaction mostly; i.e., Steckler et al., 1999; Deibert et al., 2003; Kertzhus and Kneller, 2009; Patruno et al., 2015; Klausen and Helland-Hansen, 2018), we retrieved their depositional geometries by correcting sediment thicknesses to their pre-compaction porosity according to their sand/clay ratio and vertical overburden (Allen and Allen, 2013).

We digitized the stratigraphic surfaces of the interpreted stratigraphic architecture in segments of constant slope bounded by pseudo-sections (Fig. 2a). The spatial resolution of our calculation is defined by the distance chosen between two pseudo sections (horizontal sampling distance, ΔX). To evaluate the influence of the spatial resolution on our results, we defined two end-members resolutions (100m and 1500m).

Time-depth conversion

Seismic data are available in two-way travel time seconds. We depth-converted the geometry of the stratigraphic surfaces using a two-layer velocity relationship (Fig. 2b):

$$\text{layer 1 (water - surface } s_1); Y's_{1(i)} = a \times (Ys_{1(i)}) \quad (2)$$

layer 2 (surface s_1 – surface s_2); $Y's_{2(i)} = a \times (Ys_{2(i)} - Ys_{1(i)})^2 + b \times (Ys_{2(i)} - Ys_{1(i)})$ (3)

s_1 and s_2 are the top and bottom surfaces of the considered sediment layer; $Ys_{1(i)}$ and $Ys_{2(i)}$ are the travel times (in seconds) of the intersection points between the pseudo section (i) and the considered surfaces s ; $Y's_{1(i)}$ and $Y's_{2(i)}$ are their respective depth in meters and a and b are the velocities of the considered intervals in meters per second.

In layer 1 (water), we used a 1488 m/s velocity (a). In layer 2 (the sedimentary layer), we derive a second-degree-polynomial equation from a compilation of velocities available at the wells located near the modelled cross-section (best-fit regression of check shot survey data). We defined a velocity (b) at each pseudo-section intersection (Fig. 2a). The layer is depth-converted at the intersection of each pseudo-section points ($Y's(i)$; Fig. 2b).

Sand/clay ratio estimation

For the compaction correction, we estimated the sand/clay ratio of each layer at well locations using well logs data (gamma-ray, sonic, resistivity, neutron porosity, and density) and cuttings descriptions. Wells are usually located on the shelf, thus, in the distal domains, we constrained sand/shale ratios from DSDP wells and/or seismic facies. We extrapolated sand/clay ratios linearly between wells to establish a grain-size distribution gradient within each stratigraphic interval (Fig. 2c). For this extrapolation, we used the following equation:

$$\text{for } X_{w(i+1)} > X(i) > X_{w(i)} : L_{X(i)} = \frac{L_{W(i+1)} - L_{W(i)}}{X_{W(i+1)} - X_{W(i)}} \times (X(i) - X_{W(i)}) \quad (4)$$

with $X_{w(i)}$ the location along the section of the well $W(i)$, $L_{W(i)}$ the sand/clay ratio at the well $W(i)$ and $L_{X(i)}$ the sand/clay ratio at a given position $X(i)$ at a given location along the section.

Correction of slopes and sediment thicknesses for differential compaction

To correct present-day slopes and sediment thicknesses for post-depositional compaction, we used the backstripping methods of Allen and Allen (2013) and equations in Watts and Ryan (1976) and Steckler and Watts (1978). Decompaction method is summarized in Figure 2d and consists in restoring the thicknesses of the considered strata between a reference surface R and the clinoform surface Sz , conditioned to the fact that the remaining porosity below the reference surface is negligible. The reference basal surface R can be either the infill/basement unconformity or a basin-scale stratigraphic surface (e.g. maximum flooding surface) deep enough (>2000m) for remaining porosity to be very low and thus for underlying sediments having reached their maximum compaction (Giles, 1997). For both case studies the reference level R corresponds to the Cretaceous / Cenozoic limit. We did not correct porosity for water-load. Indeed, in the proximal domain, water depth is low enough (<100m) for water-load

Accepted Article

correction to be negligible. In the distal domain (deltaic slopes and deep-sea depositional environment) paleo-water-depth estimation is difficult before decompaction. However, the stratigraphic layers in these domains are thin enough for the porosity correction to be negligible as well. After correction, we measured slope of each segment of the clinoforms between pseudo-sections (Fig. 2e).

Estimation of accumulation rates (Q_d) and diffusion coefficients (K_d)

Accumulation rates (Q_d)

We used the area of each stratigraphic layer ($A_{(i)}$) along the 2D cross-sections as a proxy of the accumulated volumes of sediment (the sum the trapezoid areas of the stratigraphic layer between pseudo-sections; Fig. 2e). Corresponding accumulation (or deposition) rates (Q_d) are then used as a proxy of sediment fluxes (i.e., the total amount of sediment which transited through the center point of each segment during the given time interval; Fig. 3). They were calculated using:

$$Q_{d(i)} = \frac{A_{Total} - A_{(i-1)} - \frac{A_{(i)}}{2}}{\Delta T} \quad (5)$$

with $Q_{d(i)}$ the accumulation rates (in km^2/kyr) at the center point of the segment of the stratigraphic layer (i), A_{Total} the restored total surface of sediment of the stratigraphic layer (in km^2), $A_{(i)}$ the surface of sediment deposited in the segment (i) (in km^2), and ΔT the duration of the stratigraphic interval (in kyr). Accumulation rates $Q_{d(i)}$ were then used to estimate diffusion coefficients (K_d) for various portions of the cross-section.

Depositional domains

We subdivided each stratigraphic layer into four or five depositional domains (Fig. 2f, Fig. 3) according to the slope and bathymetry at time of deposition (i.e., after porosity correction). The shelf (Sh) corresponds to the subaqueous marine shelf sensu Burgess and Steel (2008) and Olariu and Steel (2009). It has a low overall gradient (typically $0.01\text{--}0.02^\circ$, but as steep as 1° ; Asquith, 1970; Olariu and Steel, 2009) and is located between the shoreline and the shelf-edge break (i.e., topset-foreset rollover point of the clinoform) typically observed at bathymetries ranging from 50 to 300m (e.g., Olariu and Steel, 2009; Helland-Hansen and Hampson, 2009). The upper slope domain (US) corresponds to the foreset of the clinoforms and is bounded upslope by the shelf-edge break and downslope by the foreset-bottomset rollover point. Its bathymetry range from tens to several hundreds of meters and its slope can reach more than 10° (e.g., Patruno et al., 2015; Patruno and Helland-Hansen, 2018). The lower part of the slope (lower slope domain, LS) corresponds to the decreasing topographic gradient of the sigmoidal shape of the clinoforms. The distal (D) and abyssal plain domains

(AP) are characterized by very gentle slopes ($<1^\circ$) and bathymetries reaching several thousand meters.

Calculation of diffusion coefficients (K_d)

From the diffusion equation (eq. 1), we estimated K_d as the coefficient of the linear regression of the accumulation rates Q_d (i.e., proxy of the sedimentary fluxes) against the measured slopes (i.e. gradient) in each depositional domain (Fig. 3).

To evaluate the relevance of the diffusion-like approximation in the various depositional domains and for the different spatial and temporal scales, we also calculated the coefficient of determination R^2 of the linear regression. If the R^2 value is close to one, the accumulation rate Q_d / slope S relationship is robust and the diffusion approximation reproduces consistently transport and deposition in the depositional domain. On the other hand, if R^2 value is close to zero, the diffusion approach is not optimal to approximate sedimentary processes in the given domain or temporal or spatial scales.

Source of errors and method to estimate calculation uncertainties

Our estimation of the diffusion coefficient K_d is based on two major assumptions that are inherent to the scale and scope of the subsurface dataset used in sedimentary basin analysis.

- (i) We used accumulation rates (Q_d) as a proxy to the sediment flux. Indeed, the catchment evolution in the source areas cannot be resolved and the sediment flux has to be estimated.
- (ii) Also, we assume that sediments are deposited within the same time interval from the upstream to the downstream of the depositional profile (i.e., stratigraphic surfaces are time-lines).

Among the sources of uncertainties in our measurement are the calibration of stratigraphic surfaces in absolute ages and the estimation of the duration of their relative depositional sequences. Despite the resolutions of our age models (100 ka and 500 ka), they impact the calculations of accumulations rates and, in doing so, the estimation of the K_d . To take this effect into account in our calculations, we estimated a range of uncertainty for the age of each stratigraphic surface and included it in the calculations (Fig. 4a). The time-to-depth conversion and the sand/clay ratio impacts the geometries of stratigraphic layer via the porosity correction and estimation of depositional slopes and sediment accumulations. To take these effects into account in our calculations, we included in the calculations a range of variation of the coefficients of the second order polynomial equation used for depth conversion (Fig. 4a). We also included a 20% range of variation on the sand/shale ratios estimated from cuttings and well logs. We compiled published values of surface porosities Φ_0 and coefficients of compaction C (e.g., Bachman & Hamilton, 1976; Sclater & Christie, 1980; Baldwin & Butler, 1985; Fowler & Nisbet, 1985; Audet & Fowler, 1992; Giles, 1997; Kominz & Pekar, 2001;

Marcussen et al., 2009, 2010). We estimated overall uncertainties related to these parameters (age of stratigraphic surfaces, depth conversion, porosity correction) by performing twenty calculations for every segment. At each calculation, we randomly vary the parameters within their variation range using a normal law (Fig. 4a). Our results present the mean values of these twenty calculations. In addition, we performed the calculations with the different spatial (distance between pseudo-sections, Δx) and temporal resolutions (time increment, ΔT).

Figure 4b illustrates the mean values of deposition rates and slopes and their associated uncertainties for a given stratigraphic layer at low resolution ($\Delta x = 1500\text{m}$; $\Delta T = 500\text{ ka}$). Although significant, the minimum and maximum values remain within order of magnitude and follow the same trend. Generally, the thinner the stratigraphic layer, the higher is uncertainty on the deposition rate due to a greater impact of the age uncertainty. The uncertainties are higher on the shelf than in the rest of the depositional domains.

CASE STUDIES

We estimated diffusion coefficients from two Neogene to Quaternary (5-12 Ma) siliciclastic deltaic systems: the Ogooué delta on the West-African Gabon rifted margin and the Zambezi delta on the East-African Mozambic rifted margin (Fig. 5).

Geological setting of the Ogooué and Zambezi Deltas

The Ogooué deltaic system is located north of the N'Komi and south of the Kango and Fang transform fracture zones (TFZ; Fig. 5a). It is part of the northern Gabon offshore sub-basin and developed at a mature stage of this Cretaceous rifted margin. We chose that case study because it is relatively small (150 x 250 km) and relatively well delimited (i.e., Kango and N'Komi TFZ; Fig. 5a), its geometry is not affected by gravity driven deformation associated with evaporites and it is well covered by industrial sub-surface data. The modern Ogooué fan extends over more than 550 km westwards of the Gabonese shelf and passes through the Cameroon volcanic line (Mignard et al., 2017, 2019). Mougamba (1999) analyzed the Cenozoic stratigraphic architecture and evolution of the delta and showed a Neogene to Quaternary progradation sequence. We analyzed these Plio-Pleistocene deltaic clinoforms (last 5 Ma).

The Zambezi Delta is located along the northern Mozambican Margin which is bounded by the Mozambique TFZ to the west and the Davie Ridge or Davie TFZ to the east (Fig. 5b). The Beira High is a continental topographic structure (280 km long and 100 km wide) parallel to the coastline (König and Jokat, 2010; Mueller et al., 2016) dividing the Zambezi sedimentary system into a proximal part including the deltaic domain and the Zambezi depression, and a distal part (the Angoche Basin) corresponding to the abyssal plain associated with a major

turbiditic system and contouritic deposits related to strong oceanic circulations in this area (Diaz-Estevé and Pierce, 2017; Wiles et al., 2017; Sansom, 2018; Fierens et al., 2019; Miramontes et al., 2019; Ponte et al., 2019; Thiéblemont et al., 2019, 2020; Fig. 5b). The Zambezi delta structure is much larger (500 x 2000 km) and complex than the Ogooué delta. The Neogene sequences were determined and dated at high-resolution by Ponte et al (2019). We restored these Miocene to Pleistocene deltaic clinoforms (last 12 Ma).

Dataset

For the seismic stratigraphy analysis, we used an extensive industrial 2D seismic reflection dataset shot from the 1970's and the 2000's which has been made available by the company TotalEnergies (Fig. 5). We used five industrial exploration wells and one DSDP well (Deep Sea Drilling Project) to calibrate our seismic interpretation in terms of lithology, age and depositional environments: two wells for the Ogooué delta profile (wells O1 and O2) and three for the Zambezi delta profile (X', X2, X3) (Figs. 5 and 6).

Stratigraphic architectures

Our interpretations of the reference cross-sections of the Ogooué and Zambezi deltas in high-resolution seismic stratigraphy is based on the works of Mougamba (1999) and Ponte et al. (2019) respectively.

Both deltas show a progradational-aggradational trend during the Neogene to Quaternary (Fig. 6). The depositional profiles increased in height and steepness through time suggesting variations of the progradation rate driven by an increase of the sediment supply to the deltas. In both deltas, the upslope is flat and relatively continuous and corresponds to alternating deltaic plains and shelf deposits (calibration by well-logs and cuttings). The clinoforms show steep slopes with clayey siltstones and a wide variety of facies from gravitary deposits to hemipelagites at their base. The Zambezi delta shows (1) significant amount of gravitary deposits (from shallow turbidites lobes to Mass Transport Complex – MTC) and (2) mounded structures characteristic of the effect of oceanic currents (contourites; e.g., Faugères et al., 1999; Rebesco et al., 2014, Thiéblemont et al., 2019, 2020). For both systems, we identified several depositional sequences during the Neogene to Quaternary (Fig. 6 a2, b2): nine in the Ogooué Delta (PL-01 to PL-O9) and sixteen in the Zambezi Delta (MZ1 – MZ10 and PL.Z1 to PL.Z6).

In both deltas, most system-tracks correspond to lowstand normal regressive (LNR) deposits. They are especially well preserved in the Ogooué delta where they constitute most of the Plio-Pleistocene infilling. One period of accommodation removal is preserved in the Ogooué delta (forced regression; FR). Especially well illustrated along the Zambezi deltaic slopes, gravity flow deposits are part of the LNR and onlap the unconformity at the toe of the clinoforms.

Transgressive deposits (T) are recorded by one or a few reflectors and are sometimes completely or partly eroded by the overlying unconformity. Numerous well-preserved thin highstand normal regressive (HNR) deposits are recorded below the unconformity in the Zambezi delta and are mostly eroded by the latter in the Ogooué delta (Fig. 6 b2).

Slopes and bathymetries

In both deltas, the mean shelf slope is lower than 1.5 % except for local perturbations of the depositional profile where they can reach 5 % (Fig. 7). Paleobathymetries range from 50 to 100 m (Fig. 7). The proximal limit of the upper deltaic domain is the shelf-break which shows a great and rapid slope increase up to a mean value of 11 % and a paleo-depth of 500 m. At the transition from upper to lower deltaic domain of slope values decrease rapidly to 3-4 % with mean paleobathymetries ranging from 1000 m in the Zambezi delta to 1600-1800 m in the Ogooué delta. The distal domain and abyssal plain (only observed in the Zambezi delta) have very gentle slope (<1.5 %) and paleobathymetries ranging from 1000 to 2500 m in the Ogooué delta and over 5000 m in the Mozambique channel (Figs. 7b and 7c). For the Ogooué delta, scarcity of data in the distal and proximal deltaic domains is a source of uncertainties (Fig. 5 and 6). However, less than ≈ 10 % of the total Plio-Pleistocene volume of sediments of the Ogooué delta are deposited in these domains, reducing the impact of these uncertainties on our calculations. As a difference, the distal Zambezi delta is extremely well covered by seismic and well data (Ponte et al., 2019).

Age model

The high-resolution calibration in absolute ages of the stratigraphic surfaces is based on the approach developed by Ponte et al. (2019). It is based on biostratigraphy data (planktonic foraminifer and calcareous nanofossiles biozones) available at wells which give a resolution of several tens of thousands to million years (low resolution age model). We then improved the temporal resolution by correlating third (1-2 Myr) to fourth ($\times 0.1$ Myr) orders stratigraphic sequences with climatic and eustatic charts (e.g., Zachos et al., 2001; Lisiecki and Raymo, 2005, 2007; Miller et al., 2005; De Boer et al., 2010; Spratt and Lisiecki, 2016) assuming that higher frequency depositional sequences resulted from climate-induced sea level variations related to the Earth orbital parameters variations (i.e., Milankovich cycles; e.g. Strasser et al., 2000; Boulila et al., 2011; Laskar, 2011; Martinez and Dera, 2015; high resolution age model).

In the Ogooué delta, the mean duration of stratigraphic cycles is 0.6 Myr (low resolution age model) with system tracks estimated to represent 40 to 100 Kyr (high resolution age model; Fig.6 a3). In the Zambezi delta, the duration is 0.8 Myr for stratigraphic cycles and 40 to 100 Kyr for the system tracks in the Miocene to Pleistocene interval (Fig. 5b3).

RESULTS: DIFFUSION COEFFICIENT VARIABILITY

Diffusion coefficients K_d are determined from the mean values of regression coefficients of the depositional rate/ slope relationships (Q_d/S) estimated by twenty calculations (Fig. 8). They range from -0.18 to 0.8 km^2/ka in the Ogooué delta and -0.30 to 2 km^2/ka in the Zambezi delta (Fig.1; Fig. 9). The mean values of K_d range from 0.03 to 0.1 km^2/ka for both deltas. Most of the diffusion coefficients K_d values fall within the same order of magnitude ($\times 0.1 \text{ km}^2/\text{ka}$) which is a much narrower range than previously published values ($\times 0.0001$ to $\times 10 \text{ km}^2/\text{ka}$; Fig. 1). The best fits of the regressions are observed in the upper deltaic slope domain where slopes are steep while distal and proximal domains show more variability in K_d values. The parameters responsible for these variations are discussed hereafter.

Influence of spatial and temporal resolution

We tested for the influence of the time resolution (ΔT) and sampling distance (Δx) on the measured values of K_d and their variability (R^2). To do this, we defined two end-member combinations of temporal and spatial resolutions: (1) the High-Resolution combination (HR) with short sampling distances ($\Delta x = 0.1 \text{ km}$ for the Ogooué; $\Delta x = 0.15 \text{ km}$ for the Zambezi) and time intervals (system track scale with ΔT ca. 0.1 Ma), and, (2) the Low-Resolution combination (LR) with long sampling distances ($\Delta x = 1.5 \text{ km}$) and time intervals (depositional sequences scale with ΔT ca. 0.5 Ma; Fig. 9). For the Zambezi abyssal plain domain, which is over 2300 km long, we used longer sampling distances (HR $\Delta x = 5 \text{ km}$ and LR Δx of 25 km) and time intervals (ΔT of 2 to 6 Ma; Fig. 8). At high-resolution (HR) we measured forty-nine values in the Ogooué delta and forty-eight in the Zambezi while we measured respectively nine and sixteen values at low-resolution (LR).

The values of K_d increase with longer sampling distance (Δx) while their variability decrease (higher R^2 , Fig. 7a). The values of K_d (and their variability) decrease slightly with shorter time resolution (ΔT ; Fig. 8b). However, all K_d values remain within the same order of magnitude irrespective of the spatial and temporal resolutions.

Variation of K_d along the depositional profile

The K_d values and their dispersion vary along the depositional profile (i.e., with slopes and bathymetries; Fig. 9). K_d values are negative (-0.29 to -0.05 km^2/ka) for low bathymetries (0-200 m), low and less variable (low interquartile range, IQR and high R^2) for bathymetries ranging from 200 to 1000 m (0.05 to 0.1 km^2/ka) and higher and scattered in the deepest part (> 1000 m) of the basin (up to 1.7 km^2/ka , high IQR, low R^2 , Fig. 9b). As a consequence, the mean K_d values are negative on the shelf (ranging from -0.026 to -0.15 km^2/ka), low on the deltaic slopes (0.02 – 0.11 km^2/ka) and higher and variable in the distal domains (0.39 to 1.31

km²/ka). The best fit of the linear regression is for the upper deltaic slope domains where the slopes are the steepest (Fig. 9a).

Variation of K_d with the stratigraphic context

Regardless of the stratigraphic context (highstand or lowstand), the values of K_d range from 0.03 to 0.1 km²/ka for both deltas (white rectangles on Fig. 10). The dispersion of K_d values does however vary according to the type of system tracks (Fig. 10): it is higher for Highstand Normal Regressive system tracks (0.6 and 0.25 km²/ka for the Ogooué and Zambezi deltas respectively) than for Lowstand Normal Regressive system tracks (0.22 and 0.18 km²/ka for the Ogooué and Zambezi deltas respectively, Fig. 10). The lowest dispersion is observed for Transgressive system tracks (IQR 0.08 and 0.12 km²/ka for the Ogooué and Zambezi deltas respectively; Fig. 10). However, this may result from the limited number of measurements as these system-tracks are less preserved than the others.

Within each type of system tract, K_d values follow the same trend along the depositional profile than globally: (i) negative values for the shelf; (ii) low and moderately scattered (low IQR) values for the upper and lower deltaic slopes and (iii) higher and very variable values in distal domains (high IQR). The only exception is the Highstand Normal Regressive system tracks of the Zambezi delta where the highest K_d values are observed for the upper deltaic slopes and where distal domains show low K_d variations (IQR= 0.12; Fig. 10). The scattered values for the Ogooué Highstand Normal Regressive system tracks results from the limited number of measurements (n=2; Fig. 10 a2).

This statistical analysis shows that K_d values are independent of the stratigraphic context that is to say independent of the accommodation / sedimentation ratio driving the stratigraphic sequences.

Variation of K_d through time

The slope S and accumulation rate Q_d values of the stratigraphic intervals of the Ogooué and Zambezi deltas are fairly constant through time within each depositional domain (Fig. 11). More variability is nonetheless observed at high resolution (Fig. 11). K_d values range within the same order of magnitude except on the shelf and, rarely, on the lower slopes and distal domain where negative values are calculated.

Nevertheless, in the Zambezi delta, two moderate K_d values increases along with Q_d values at the upper Tortonian (8 Ma) and the Messinian/Zanclean (c. 5.3 Ma) boundary. In the Ogooué delta, K_d values increase in the distal domain at the Pliocene-Pleistocene transition (c. 2.6 Ma) along with significant increase of the values of slopes (particularly in the upper deltaic slope domain) and Q_d . Following a decrease during the Gelasian, K_d values increase in both deltas

during the Calabrian, especially after 0.9 Ma. This increase is coeval of an increase of Q_d while the slopes remain fairly constant.

DISCUSSIONS

Causes of diffusion coefficient variations

The diffusion coefficients K_d values we calculated fall within the same order of magnitude ($\times 0,1 \text{ km}^2/\text{ka}$) which is a much narrower range than previously published values ($\times 0,0001$ to $\times 10 \text{ km}^2/\text{ka}$; Fig. 1). This narrow range values indicates that, at first order, the flux is compensated by the slope along the depositional profile.

Our statistical analysis shows that the diffusion is optimal to approximate sediment transport and deposition across rifted margins at a kilometric scale and for time intervals of 0.5 – 1Ma. At these scales, the assumption that sediments are transported proportionally to the slope, consistently averages the various sedimentary processes occurring within the different domains of the depositional profile.

Nevertheless, within this narrow range, we documented variations of K_d values that suggest that the flux/slope ratio evolves along the depositional profile (Fig. 12). The best fit of the linear regression is in the upper deltaic slope domain where steep slopes are consistent with gravitary transport, i.e., the process is approximated by diffusion (Fig. 12). The negative values on the shelf are the results of local disturbance in the deposition gradient by proximal sedimentary processes (e.g., waves, tides, or shore and littoral drift; Fig. 12). The diffusion is therefore not optimal to approximate transport and deposition on the shelf at kilometric scale and for million years time intervals. Similarly, the variability of K_d values in distal domains results from gentle slopes and changes in sedimentary flux values and directions controlled by sedimentary processes such as hemipelagic deposition, turbiditic events and oceanic currents. The diffusion is therefore not optimal to approximate transport and deposition in the distal domain either (Fig. 12). Furthermore, the low values of the coefficients of determination of the linear regression in the distal domain also suggest a non-linear relation between the slope and the accumulations rates in this part of the depositional profile.

The lack of relationship between K_d values and the stratigraphic context implies that the variations of the accommodation and sedimentation ratio, driving the sequence stratigraphic framework, do not affect the K_d values. Thus, at kilometric and 1 Ma scales, variations in sediment flux are compensated by variation of slopes along the depositional profile: the slope become steeper during progradation than during retrogradation in both the Ogooué and Zambezi deltas.

Effect of tectonic and climate on sedimentation dynamic

An increase in sediment supply to a rifted margin basins may result from relief variations in the drainage areas of the deltas that may result from increase either in rock-uplift or in climate-driven erosion efficiency, or both. The stratigraphic record of an uplift in the drainage area of rifted margin has three distinct signatures: (1) a tilting of the margin stratigraphic horizons truncated by an angular unconformity, (2) a major relative sea-level fall and (3) an increase in siliciclastic sediment supply (if humid conditions prevailed).

At the Piacenzian/Gelasian boundary, the uplift of the rifted margin of the Zambezi delta is suggested by a relative sea-level fall and a sharp downward shift of the shoreline (forced regression; Ponte et al 2019; Fig. 5). This may have caused the increase of the slope, Q_d and K_d that we documented at this time (Fig. 11). In the Late Tortonian and at the Messinian/Zanclean boundary, the increase in Q_d and K_d values recorded in the Zambezi delta (Fig. 11) may have recorded an increase in uplift rate in the drainage area, a major climate change and/or a drainage reorganization. Other observations are needed to decipher the cause(s).

In addition, both deltas record an increase of Q_d and K_d values at 0.9 Ma (Fig. 11). This increase is coeval of an increase in the amplitude of eustatic variations at this time (Middle Pleistocene Transition; Hansen et al., 2013; Miller et al., 2020; Fig. 11). Nevertheless, the Ogooué delta also records a decrease of Q_d and K_d values after 0.4 Ma (Fig. 11). There is no indication of change in the drainage area over that period (Guillocheau et al., 2015), nor of a change in the amplitude of the eustatic variations. This suggest that this decrease in Q_d (and K_d) values may have been controlled by a change in the type of climate. Accordingly, the durations of the glacial and interglacial phases evolve in favor of the glacial phases over the last 0.8 Ma (Past Interglacials Working Group of PAGES, 2016), and in doing so, in favor of a more arid climate (e.g. Rommerskirchen et al., 2006).

These observations suggest a temporal correlation between climate and tectonic variations on the sedimentary supply to rifted margin deltas. However, additional models and studies varying precipitations and erodibility are needed to further explore of the relative effect of climate and tectonic on sedimentary flux.

Limits of K_d estimation on natural systems

We estimated the variability of the diffusion coefficients associated with uncertainties in every step of the calculation (e.g., calibration in absolute ages, time-depth conversion, sand/shale ratio and porosity correction). At first order, the adequacy of the diffusion approximation is most of all limited by sedimentary processes (waves, hemipelagites and carbonates, turbiditic and oceanic currents) altering slopes and fluxes (both in values and directions) on the shelf and in the distal domains, and in doing so, the measured K_d . These processes are therefore not

Accepted Article

optimally approximated by diffusion with a constant transport coefficient. This is why, in some numerical simulations, authors have chosen to vary coefficients as a function of the water depth (e.g. Paola, 2000), which highlights the limit of linear diffusion as an all-in-one solution to reproduce the whole complexity of natural systems.

Furthermore, our measurements were performed for two sedimentary systems formed during the Pliocene - Pleistocene icehouse. In this climatic context of high-frequency/high-amplitude changes in absolute sea level, the stratigraphic record is characterized by specific patterns of sediment distribution and chronostratigraphic relationships. These fairly “modern” relationships are often used as a template for sequence stratigraphic interpretation and predicting sediment distribution of pre-Pliocene sedimentary systems potentially formed during greenhouse climatic context when absolute sea-level fluctuations are known to have been different. Care should therefore be taken when extrapolating calibrations performed on icehouse driven sedimentary systems to greenhouse driven systems which may have different dynamics.

Finally, our measurements were only performed for two rifted margin deltas and additional measurements in distinct geological settings (e.g., foreland, rift) are necessary to define a comprehensive range of reasonable diffusion coefficient values.

CONCLUSIONS

We developed a methodology to estimate diffusion coefficients from the flux / slope ratio along the depositional profiles of sedimentary systems using high resolution seismic stratigraphy analysis of their stratigraphic architecture. We applied the method to two natural examples of rifted margin shelf-edge deltas. For each stratigraphic sequence, (1) we calibrated the sand/shale ratios across the depositional profile in order to (2) restore the depositional slope of each stratigraphic horizon by correcting for post-depositional compaction. (3) We then estimated uncompacted accumulated volumes in order to estimate (4) the transport coefficient K_d from the ratio of the sediment flux and the slope.

The measured values of diffusion coefficients fall within a single order of magnitude ($\times 0,1 \text{ km}^2/\text{ka}$) irrespective of the stratigraphic context or the sand/clay ratio. Our statistical analysis shows that the diffusion is optimal to approximate sedimentary processes at kilometeric scale and for time intervals of 500 ka – 1 Ma. The diffusion coefficient values vary according to the depositional domain. The diffusion assumption is optimal for the deltaic slope domain where slopes are steep and mostly controlled by gravity-driven transport. On the platform and in the distal domain, other sedimentary processes such as oceanic currents, turbiditic channels, hemipelagites, or waves limit the relevance of the diffusion approximation. We show that the diffusion coefficients values and the sedimentary flux increase at 0.9 Ma along with an increase in the amplitude of eustatic variations. This highlights the interplay between

catchment dynamics, sedimentary supply and offshore sediment transport. This also indicates that the calibration of diffusion coefficient from present day sedimentary systems might not be optimal for simulations of systems deposited before the Pliocene.

REFERENCES

- Allen, P. A., and Allen, J. R. (2013). *Basin analysis: Principles and application to petroleum play assessment* (Third edit). Wiley-Blackwell.
- Audet, D., and Fowler, A. (1992). A mathematical model for compaction in sedimentary basins. *Geophysical Journal International*, 110(3), 577–590.
- Bachman, R. T., and Hamilton, E. L. (1976). Density, porosity, and grain density of samples from Deep Sea Drilling Project Site 222 (Leg 23) in the Arabian Sea. *Journal of Sedimentary Research*, 46(3), 654–658.
- Baldwin, B., & Butler, C. O. (1985). Compaction curves. *AAPG Bulletin*, 69(4), 622–626.
- Begin, Z. B., Meyer, D. F., and Schumm, S. A. (1981). Development of longitudinal profiles of alluvial channels in response to base-level lowering. *Earth Surface Processes and Landforms*, 6(1), 49–68.
- Boulila, S., Galbrun, B., Miller, K. G., Pekar, S. F., Browning, J. V., Laskar, J., and Wright, J. D. (2011). On the origin of Cenozoic and Mesozoic “third-order” eustatic sequences. *Earth-Science Reviews*, 109(3–4), 94–112.
- Bowman, S. A., and Vail, P. R. (1993). Carbonate sedimentation process. *Am. Assoc. Pet. Geol., Annu. Conv. Progr*, 78.
- Braun, J., and Willett, S. D. (2013). A very efficient $O(n)$, implicit and parallel method to solve the stream power equation governing fluvial incision and landscape evolution. *Geomorphology*, 180, 170–179.
- Bullimore, S., Henriksen, S., Liestøl, F. M., and Helland-Hansen, W. (2005). Clinoform stacking patterns, shelf-edge trajectories and facies associations in Tertiary coastal deltas, offshore Norway: Implications for the prediction of lithology in prograding systems. *Norwegian Journal of Geology/Norsk Geologisk Forening*, 85.
- Burgess, P. M., Lammers, H., van Oosterhout, C., and Granjeon, D. (2006). Multivariate sequence stratigraphy: Tackling complexity and uncertainty with stratigraphic forward modeling, multiple scenarios, and conditional frequency maps. *AAPG Bulletin*, 90(12), 1883–1901. <https://doi.org/10.1306/06260605081>
- Burgess, P. M., and Prince, G. D. (2015). Non-unique stratal geometries: Implications for sequence stratigraphic interpretations. *Basin Research*, 27(3), 351–365.
- Burgess, P. M., Roberts, D., and Bally, A. (2012). A brief review of developments in stratigraphic forward modelling, 2000–2009. *Regional Geology and Tectonics: Principles of Geologic Analysis*, 1, 379–404.
- Candido, M., Cagliari, J., Tognoli, F. M. W., and Lavina, E. L. C. (2019). Stratigraphic modeling of a transgressive barrier-lagoon in the Permian of Paraná Basin, southern Brazil. *Journal of South American Earth Sciences*, 90, 377–391.
- Carson, M. A., and Kirkby, M. J. (1972). Hillslope form and process. In *Cambridge Geographical Studies* (Vol. 3, p. 475). Cambridge Univ. Press.
- Carvajal, C. R., and Steel, R. J. (2009). Shelf-edge architecture and bypass of sand to deep water; influence of shelf-edge processes, sea level, and sediment supply. *Journal of Sedimentary Research*, 79(9), 652–672.
- Clark, S., Bruaset, A., Sømme, T., and Løseth, T. (2009). *A flexible stochastic approach to constraining uncertainty in forward stratigraphic models*. presented at the MODSIM09 Int. Congr. Modell. Simulat.
- Coulthard, T. J., Kirkby, M. J., and Macklin, M. G. (2000). Modelling geomorphic response to environmental change in an upland catchment. *Hydrological Processes*, 14(11-12), 2031 –

2045.

Cross, T. A., and Lessenger, M. A. (1999). Construction and application of a stratigraphic inverse model. In J. W. Hardbaugh, W. L. Watney, E. C. Rankey, Slingerland, and R. H. Goldstein (Eds.), *Numerical Experiments in Stratigraphy: Recent Advances in Stratigraphic and Sedimentologic Computer Simulations*. Special Publications of SEPM.

Csato, I., Catuneanu, O., and Granjeon, D. (2014). Millennial-scale sequence stratigraphy; numerical simulation with Dionisos. *Journal of Sedimentary Research*, 84(5), 394–406. <https://doi.org/10.2110/jsr.2014.36>

Csato, I., Granjeon, D., Catuneanu, O., and Baum, G. R. (2012). A three-dimensional stratigraphic model for the Messinian crisis in the Pannonian Basin, eastern Hungary. *Basin Research*, 25(2), 121–148.

Csato, I., Kendall, C. G. S. C., and Moore, P. D. (2007). The Messinian problem in the Pannonian Basin, Eastern Hungary—Insights from stratigraphic simulations. *Sedimentary Geology*, 201(1–2), 111–140.

Culling, W. E. H. (1960). Analytical theory of erosion. *The Journal of Geology*, 336–344.

De Boer, B., Van de Wal, R., Bintanja, R., Lourens, L., and Tuenter, E. (2010). Cenozoic global ice-volume and temperature simulations with 1-D ice-sheet models forced by benthic $\delta^{18}\text{O}$ records. *Annals of Glaciology*, 51(55), 23–33.

Deibert, J. E., Benda, T., Løseth, T., Schellpeper, M., and Steel, R. J. (2003). Eocene clinoform growth in front of a storm-wave-dominated shelf, Central Basin, Spitsbergen: No significant sand delivery to deepwater areas. *Journal of Sedimentary Research*, 73(4), 546–558.

Diaz-Esteve, A., and Pierce, A. (2017). *Contourites as a Primary Regional Control on Deep-Water Sediment Deposition: Examples from the Mozambique Basin*. 2017(1), 1–3.

Ding, X., Salles, T., Flament, N., and Rey, P. (2019). Quantitative stratigraphic analysis in a source-to-sink numerical framework. *Geoscientific Model Development*, 12(6), 2571–2585.

Euzen, T., Joseph, P., du Fornel, E., Lesur, S., Granjeon, D., and Guillocheau, F. (2004). Three-dimensional stratigraphic modelling of the Gres d'Annot system, Eocene-Oligocene, SE France. *Geological Society Special Publications*, 221, 161–180.

Fierens, R., Droz, L., Toucanne, S., Raison, F., Jouet, G., Babonneau, N., Miramontes, E., Landurain, S., and Jorry, S. J. (2019). Late Quaternary geomorphology and sedimentary processes in the Zambezi turbidite system (Mozambique Channel). *Geomorphology*, 334, 1–28.

Flemings, P. B., and Jordan, T. E. (1989). A synthetic stratigraphic model of foreland basin development. *Journal of Geophysical Research: Solid Earth*, 94(B4), 3851–3866.

Fowler, C., and Nisbet, E. (1985). The subsidence of the Williston Basin. *Canadian Journal of Earth Sciences*, 22(3), 408–415.

Giles, M. R. (1997). *Diagenesis: A quantitative perspective: Implications for basin modelling and rock property prediction*. Springer.

Glørstad-Clark, E., Faleide, J. I., Lundschie, B. A., and Nystuen, J. P. (2010). Triassic seismic sequence stratigraphy and paleogeography of the western Barents Sea area. *Marine and Petroleum Geology*, 27(7), 1448–1475.

Granjeon, D. (1996). Modelisation stratigraphique deterministe; conception et applications d'un modele diffusif 3D multilithologique [PhD Thesis, Geosciences Rennes : Rennes, France]. In *Deterministic stratigraphic modelling; conception and applications of a multi-lithologic 3D model* (Vol. 78).

Granjeon, D. (2014). 3D forward modelling of the impact of sediment transport and level cycles on continental margins and incised valleys. *Special Publication of the International Association*

of *Sedimentologists*, 46, 453–472.

Granjeon, D., and Joseph, P. (1999). Concepts and applications of a 3-D multiple lithology, diffusive model in stratigraphic modeling. *Special Publication - Society for Sedimentary Geology*, 62, 197–210.

Guillocheau, F., Chelalou, R., Linol, B., Dauteuil, O., Robin, C., Mvondo, F., Callec, Y., and Colin, J. P. (2015). Cenozoic landscape evolution in and around the Congo Basin: Constraints from sediments and planation surfaces. In *Geology and resource potential of the Congo Basin* (pp. 271-313). Springer, Berlin, Heidelberg.

Hansen, J., Sato, M., Russell, G., and Kharecha, P. (2013). Climate sensitivity, sea level and atmospheric carbon dioxide. *Philosophical Transactions of the Royal Society - A: Mathematical, Physical and Engineering Sciences*, 371(2001), 20120294.

Harris, A. D., Carvajal, C., Covault, J., Perlmutter, M., and Sun, T. (2015). Numerical stratigraphic modeling of climatic controls on basin-scale sedimentation. *AAPG Annual Convention and Exhibition*, 31.

Harris, A. D., Covault, J. A., Madof, A. S., Sun, T., Sylvester, Z., and Granjeon, D. (2016). Three-dimensional numerical modeling of eustatic control on continental-margin sand distribution. d. Harris et al. Numerical modeling of eustatic control on continental-margin sand distribution. *Journal of Sedimentary Research*, 86(12), 1434–1443.

Hawie, N., Barrois, A., Marfisi, E., Murat, B., Hall, J., El-Wazir, Z., Al-Madani, N., and Aillud, G. (2015). *Forward stratigraphic modelling, deterministic approach to improve carbonate heterogeneity prediction; lower cretaceous, Abu Dhabi*. Abu Dhabi International Petroleum Exhibition and Conference.

Helland-Hansen, W., and Gjelberg, J. G. (1994). Conceptual basis and variability in sequence stratigraphy: A different perspective. *Sedimentary Geology*, 92(1–2), 31–52.

Helland-Hansen, W., and Hampson, G. J. (2009). Trajectory analysis: Concepts and applications. *Basin Research*, 21(5), 454–483. <https://doi.org/10.1111/j.1365-2117.2009.00425.x>

Helland-Hansen, W., and Martinsen, O. J. (1996). Shoreline trajectories and sequences; description of variable depositional-dip scenarios. *Journal of Sedimentary Research*, 66(4), 670–688.

Herman, F., and Champagnac, J. (2016). Plio-Pleistocene increase of erosion rates in mountain belts in response to climate change. *Terra Nova*, 28(1), 2–10.

Herman, F., Seward, D., Valla, P. G., Carter, A., Kohn, B., Willett, S. D., and Ehlers, T. A. (2013). Worldwide acceleration of mountain erosion under a cooling climate. *Nature*, 504(7480), 423–426.

Houston, W. S., Huntoon, J. E., and Kamola, D. L. (2000). Modeling of Cretaceous foreland-basin parasequences, Utah, with implications for timing of Sevier thrusting. *Geology*, 28(3), 267–270.

Hutton, E. W. H., and Syvitski, J. P. M. (2008). Sedflux 2.0: An advanced process-response model that generates three-dimensional stratigraphy. *Computers and Geosciences*, 34(10), 1319–1337.

Johannessen, E. P., and Steel, R. J. (2005). Shelf-margin clinoforms and prediction of deepwater sands. *Basin Research*, 17(4), 521–550.

Jordan, T. E., and Flemings, P. B. (1991). Large-scale stratigraphic architecture, eustatic variation, and unsteady tectonism: A theoretical evaluation. *Journal of Geophysical Research: Solid Earth*, 96(B4), 6681–6699.

Kaufman, P., Grotzinger, J. P., and McCormick, D. S. (1991). Depth-dependent diffusion

algorithm for simulation of sedimentation in shallow marine depositional systems. *Kansas Geological Survey Bulletin*, 233, 489–508.

Kendall, C. G. S. C., Strobel, J., Cannon, R., Bezdek, J., and Biswas, G. (1991). The simulation of the sedimentary fill of basins. *Journal of Geophysical Research: Solid Earth*, 96(B4), 6911–6929.

Kenyon, P. M., and Turcotte, D. L. (1985). Morphology of a delta prograding by bulk sediment transport. *Geological Society of America Bulletin*, 96(11), 1457–1465.

Kertzus, V., and Kneller, B. (2009). Clinoform quantification for assessing the effects of external forcing on continental margin development. *Basin Research*, 21(5), 738–758.

Klausen, T. G., and Helland-Hansen, W. (2018). Methods for restoring and describing ancient clinoform surfaces. *Journal of Sedimentary Research*, 88(2), 241–259.

Kolodka, C., Vennin, E., Bourillot, R., Granjeon, D., and Desaubliaux, G. (2016). Stratigraphic modelling of platform architecture and carbonate production: A Messinian case study (Sorbas Basin, SE Spain). *Basin Research*, 28(5), 658–684.

Kominz, M. A., and Pekar, S. F. (2001). Oligocene eustasy from two-dimensional sequence stratigraphic backstripping. *Geological Society of America Bulletin*, 113(3), 291–304.

König, M., and Jokat, W. (2010). Advanced insights into magmatism and volcanism of the Mozambique Ridge and Mozambique Basin in the view of new potential field data. *Geophysical Journal International*, 180(1), 158–180.

Leroux, E. (2012). *Quantification des flux sédimentaires et de la subsidence du bassin Provençal* [PhD Thesis, Université de Bretagne Occidentale].

Leroux, E., Rabineau, M., Aslanian, D., Granjeon, D., Droz, L., and Gorini, C. (2014). Stratigraphic simulations of the shelf of the Gulf of Lions; testing subsidence rates and sea-level curves during the Pliocene and Quaternary. *Terra Nova*, 26(3), 230–238. <https://doi.org/10.1111/ter.12091>

Lisiecki, L. E., and Raymo, M. E. (2005). A Pliocene-Pleistocene stack of 57 globally distributed benthic $\delta^{18}\text{O}$ records. *Paleoceanography*, 20(1).

Lisiecki, L. E., and Raymo, M. E. (2007). Plio–Pleistocene climate evolution: Trends and transitions in glacial cycle dynamics. *Quaternary Science Reviews*, 26(1–2), 56–69.

Marcussen, Ø., Maast, T. E., Mondol, N. H., Jahren, J., and Bjørlykke, K. (2010). Changes in physical properties of a reservoir sandstone as a function of burial depth—The Eivie Formation, northern North Sea. *Marine and Petroleum Geology*, 27(8), 1725–1735.

Marcussen, Ø., Thyberg, B. I., Peltonen, C., Jahren, J., Bjørlykke, K., and Faleide, J. I. (2009). Physical properties of Cenozoic mudstones from the northern North Sea: Impact of clay mineralogy on compaction trends. *AAPG Bulletin*, 93(1), 127–150.

Martinez, M., and Dera, G. (2015). Orbital pacing of carbon fluxes by a ~ 9-My eccentricity cycle during the Mesozoic. *Proceedings of the National Academy of Sciences*, 112(41), 12604–12609.

Martinez, P. A., and Harbaugh, J. W. (1993). *Simulating nearshore sedimentation*. Oxford, Pergamon.

Mignard, S. L. A., Mulder, T., Martinez, P., Charlier, K., Rossignol, L., and Garlan, T. (2017). Deep-sea terrigenous organic carbon transfer and accumulation: Impact of sea-level variations and sedimentation processes off the Ogooue River (Gabon). *Marine and Petroleum Geology*, 85, 35–53.

Mignard, S., Mulder, T., Martinez, P., and Garlan, T. (2019). The Ogooue Fan (offshore Gabon): a modern example of deep-sea fan on a complex slope profile. *Solid Earth*, 10(3), 851–869.

Miller, K. G., Kominz, M. A., Browning, J. V., Wright, J. D., Mountain, G. S., Katz, M. E., Sugarman, P. J., Cramer, B. S., Christie-Blick, N., and Pekar, S. F. (2005). The Phanerozoic record of global sea-level change. *Science*, *310*(5752), 1293–1298.

Miller, K. G., Browning, J. V., Schmelz, W. J., Kopp, R. E., Mountain, G. S., and Wright, J. D. (2020). Cenozoic sea-level and cryospheric evolution from deep-sea geochemical and continental margin records. *Science advances*, *6*(20), eaaz1346.

Miramontes, E., Penven, P., Fierens, R., Droz, L., Toucanne, S., Jorry, S. J., Jouet, G., Pastor, L., Jacinto, R. S., and Gaillot, A. (2019). The influence of bottom currents on the Zambezi Valley morphology (Mozambique Channel, SW Indian Ocean): In situ current observations and hydrodynamic modelling. *Marine Geology*, *410*, 42–55.

Mitchell, N. C. (1996). Creep in pelagic sediments and potential for morphologic dating of marine fault scarps. *Geophysical Research Letters*, *23*(5), 483–486.

Mitchell, N. C., and Huthnance, J. M. (2008). Oceanographic currents and the convexity of the uppermost continental slope. *Journal of Sedimentary Research*, *78*(1), 29–44.

Mitchum, R. M., Vail, P. R., and Sangree, J. B. (1977). Seismic Stratigraphy and Global Changes of Sea Level, Part 6: Stratigraphic Interpretation of Seismic Reflection Patterns in Depositional Sequences. In *AAPG Memoir 26 Seismic Stratigraphy—Applications to Hydrocarbon Exploration*.

Mueller, C. O., Jokat, W., and Schreckenberger, B. (2016). The crustal structure of Beira High, central Mozambique—Combined investigation of wide-angle seismic and potential field data. *Tectonophysics*, *683*, 233–254.

Murray, A. B., and Paola, C. (1994). *A cellular model of braided rivers*.

Olariu, C., and Steel, R. J. (2009). Influence of point-source sediment-supply on modern shelf-slope morphology: Implications for interpretation of ancient shelf margins. *Basin Research*, *21*(5), 484–501.

Overeem, I., Syvitski, J. P. M., and Hutton, E. W. H. (2005). Three-dimensional numerical modeling of deltas. In L. Giosan and J. P. Bhattacharya (Eds.), *River Deltas: Concepts, Models and Examples* (SEPM Speci, Vol. 83, pp. 13–30). SEPM Special Publication.

Paola, C. (2000). Quantitative models of sedimentary basin filling. *Sedimentology*, *47*(s1), 121–178.

Parker, G., Paola, C., Whipple, K. X., and Mohrig, D. (1998). Alluvial fans formed by channelized fluvial and sheet flow. I: Theory. *Journal of Hydraulic Engineering*, *124*(10), 985–995.

Past Interglacials Working Group of PAGES. (2016). Interglacials of the last 800,000 years. *Reviews of Geophysics*, *54*(1), 162–219.

Patrino, S., Hampson, G. J., and Jackson, C. A. (2015). Quantitative characterisation of deltaic and subaqueous clinoforms. *Earth-Science Reviews*, *142*, 79–119.

Pirmez, C., Pratson, L. F., and Steckler, M. S. (1998). Clinoform development by advection-diffusion of suspended sediment: Modeling and comparison to natural systems. *Journal Of Geophysical Research-All Series*, *103*, 24–141.

Ponte, J.-P., Robin, C., Guillocheau, F., Popescu, S., Suc, J.-P., Dall’Asta, M., Melinte-Dobrinescu, M. C., Bubik, M., Dupont, G., and Gaillot, J. (2019). The Zambezi delta (Mozambique channel, East Africa): High resolution dating combining bio-orbital and seismic stratigraphies to determine climate (palaeoprecipitation) and tectonic controls on a passive margin. *Marine and Petroleum Geology*, *105*, 293–312.

Posamentier, H. W., and Allen, G. P. (1993). Variability of the sequence stratigraphic model: Effects of local basin factors. *Sedimentary Geology*, *86*(1–2), 91–109.

Quiquerez, A., Allemand, P., and Dromart, G. (2000). DIBAFILL: a 3-D two-lithology diffusive model for basin infilling. *Computers and Geosciences*, 26(9–10), 1029–1042.

Reynolds, D. J., Steckler, M. S., and Coakley, B. J. (1991). The role of the sediment load in sequence stratigraphy: The influence of flexural isostasy and compaction. *Journal of Geophysical Research: Solid Earth*, 96(B4), 6931–6949.

Rich, J. L. (1951). Three critical environments of deposition, and criteria for recognition of rocks deposited in each of them. *Geological Society of America Bulletin*, 62(1), 1–20.

Ritchie, B. D., Gawthorpe, R. L., and Hardy, S. (2004a). Three-dimensional numerical modeling of deltaic depositional sequences 1: Influence of the rate and magnitude of sea-level change. *Journal of Sedimentary Research*, 74(2), 203–220.

Ritchie, B. D., Gawthorpe, R. L., and Hardy, S. (2004b). Three-dimensional numerical modeling of deltaic depositional sequences 2: Influence of local controls. *Journal of Sedimentary Research*, 74(2), 221–238.

Ritchie, B. D., Hardy, S., and Gawthorpe, R. L. (1999). Three-dimensional numerical modeling of coarse-grained clastic deposition in sedimentary basins. *Journal of Geophysical Research: Solid Earth*, 104(B8), 17759–17780.

Rivenaes, J. C. (1992). Application of a dual-lithology, depth-dependent diffusion equation in stratigraphic simulation. *Basin Research*, 4(2), 133–146.

Rivenaes, J. C. (1997). Impact of sediment transport efficiency on large-scale sequence architecture: Results from stratigraphic computer simulation. *Basin Research*, 9(2), 91–105.

Rohais, S., Eschard, R., Ford, M., Guillocheau, F., and Moretti, I. (2007). Stratigraphic architecture of the Plio-Pleistocene infill of the Corinth Rift: Implications for its structural evolution. *Tectonophysics*, 440(1–4), 5–28.

Rommerskirchen, F., Condon, T., Mollenhauer, G., Dupont, L., & Schefuss, E. (2011). Miocene to Pliocene development of surface and subsurface temperatures in the Benguela Current system. *Paleoceanography*, 26(3), PA3216.

Ross, W. C., Halliwell, B. A., May, J. A., Watts, D. E., and Syvitski, J. P. M. (1994). Slope readjustment: A new model for the development of submarine fans and aprons. *Geology*, 22(6), 511–514.

Rouby, D., Braun, J., Robin, C., Dauteuil, O., and Deschamps, F. (2013). Long-term stratigraphic evolution of Atlantic-type passive margins: A numerical approach of interactions between surface processes, flexural isostasy and 3D thermal subsidence. *Tectonophysics*, 604, 83–103.

Salles, T. (2016). Badlands: A parallel basin and landscape dynamics model. *SoftwareX*, 5, 195–202.

Salles, T., Ding, X., and Brocard, G. (2018). pyBadlands: A framework to simulate sediment transport, landscape dynamics and basin stratigraphic evolution through space and time. *PLoS One*, 13(4), e0195557.

Salles, T., Ding, X., Webster, J. M., Vila-Concejo, A., Brocard, G., and Pall, J. (2018). A unified framework for modelling sediment fate from source to sink and its interactions with reef systems over geological times. *Scientific Reports*, 8(1), 1–11.

Salles, T., and Hardiman, L. (2016). Badlands: An open-source, flexible and parallel framework to study landscape dynamics. *Computers and Geosciences*, 91, 77–89.

Sansom, P. (2018). Hybrid turbidite–contourite systems of the Tanzanian margin. *Petroleum Geoscience*, 24(3), 258–276.

Sclater, J. G., & Christie, P. A. (1980). Continental stretching: An explanation of the post-mid-Cretaceous subsidence of the central North Sea basin. *Journal of Geophysical Research: Solid Earth*, 85(B7), 3711-3739.

Spratt, R. M., and Lisiecki, L. E. (2016). A Late Pleistocene sea level stack. *Climate of the Past*, 12(4), 1079–1092.

Steckler, M. S., & Watts, A. B. (1978). Subsidence of the Atlantic-type continental margin off New York. *Earth and planetary science letters*, 41(1), 1-13.

Steckler, M. S., Mountain, G. S., Miller, K. G., and Christie-Blick, N. (1999). Reconstruction of Tertiary progradation and clinoform development on the New Jersey passive margin by 2-D backstripping. *Marine Geology*, 154(1), 399–420.

Steckler, M. S., Reynolds, D. J., Coakley, B. J., Swift, B. A., and Jarrard, R. (1993). Modelling passive margin sequence stratigraphy. *Sequence Stratigraphy and Facies Associations*, 19–41.

Steel, R., and Olsen, T. (2002). Clinoforms, clinoform trajectories and deepwater sands. *Program and Abstracts - Society of Economic Paleontologists. Gulf Coast Section. Research Conference*, 22, 367–380.

Strasser, A., Hillgärtner, H., Hug, W., and Pittet, B. (2000). Third-order depositional sequences reflecting Milankovitch cyclicity. *Terra Nova*, 12(6), 303–311.

Strobel, J., Cannon, R., Christopher, G. S., Kendall, C. S., Biswas, G., and Bezdek, J. (1989). Interactive (SEDDPAK) simulation of clastic and carbonate sediments in shelf to basin settings. *Computers and Geosciences*, 15(8), 1279–1290.

Syvitski, J. P. M., and Alcott, J. M. (1995). RIVER3: Simulation of river discharge and sediment transport. *Computers and Geosciences*, 21(1), 89–151.

Syvitski, J. P. M., and Daughney, S. (1992). DELTA2: Delta progradation and basin filling. *Computers and Geosciences*, 18(7), 839–897.

Syvitski, J. P. M., and Hutton, E. W. H. (2001). 2d sedflux 1.0 c: An advanced process-response numerical model for the fill of marine sedimentary basins. *Computers and Geosciences*, 27(6), 731–753.

Syvitski, J. P. M., Smith, J. N., Calabrese, E., and Boudreau, B. (1988). Basin sedimentation and the growth of prograding deltas. *Journal of Geophysical Research: Oceans*, 93(C6), 6895–6908.

Tetzlaff, D., and Priddy, G. (2001). Sedimentary process modeling: From academia to industry. In *Geologic modeling and simulation* (pp. 45–69). Springer.

Thiéblemont, A., Hernández-Molina, F. J., Miramontes, E., Raison, F., and Penven, P. (2019). Contourite depositional systems along the Mozambique channel: The interplay between bottom currents and sedimentary processes. *Deep Sea Research Part I: Oceanographic Research Papers*, 147, 79–99.

Thiéblemont, A., Hernandez-Molina, F. J., Ponte, J.-P., Robin, C., Guillocheau, F., Cazzola, C., and Raison, F. (2020). Seismic stratigraphic framework and depositional history for Cretaceous and Cenozoic contourite depositional systems of the Mozambique Channel, SW Indian Ocean. *Marine Geology*, 425, 106192.

Thorne, J. A., and Swift, D. J. P. (1991). Sedimentation on continental margins, VI: a regime model for depositional sequences, their component systems tracts, and bounding surfaces. In *Shelf sand and sandstone bodies: Geometry, facies and sequence stratigraphy* (Vol. 14, pp. 189–255). International Association of Sedimentologists, Special Publications.

Tiedemann, R., Sarinthein, M., and Shackleton, N. J. (1994). Astronomic timescale for the Pliocene Atlantic $\delta^{18}O$ and dust flux records of Ocean Drilling Program Site 659.

Paleoceanography, 9(4), 619–638.

Tucker, G. E., and Slingerland, R. L. (1994). Erosional dynamics, flexural isostasy, and long-lived escarpments: A numerical modeling study. *Journal of Geophysical Research: Solid Earth*, 99(B6), 12229–12243.

Vail, P. R., Mitchum, R. M., and Thompson, S. I. (1977). Seismic stratigraphy and global changes of sea level: Part 3, Relative changes of sea level from coastal onlap. In *Seismic Stratigraphy—Applications to Hydrocarbon Exploration* (63–81). American Association of Petroleum Geologists.

Wehr, F. L. (1993). Effects of Variations in Subsidence and Sediment Supply on Parasequence Stacking Patterns: Chapter 14: Recent Developments in Siliciclastic Sequence Stratigraphy. In F. Weimer and H. W. Posamentier (Eds.), *Siliclastic Sequence Stratigraphy: Recent Developments and Applications* (Vol. 58, pp. 369–379). American Association of Petroleum Geologists Memoir.

Wiles, E., Green, A., Watkeys, M., and Jokat, W. (2017). Zambezi continental margin: Compartmentalized sediment transfer routes to the abyssal Mozambique Channel. *Marine Geophysical Research*, 38(3), 227–240.

Yuan, X. P., Braun, J., Guerit, L., Simon, B., Bovy, B., Rouby, D., Robin, C., and Jiao, R. (2019). Linking continental erosion to marine sediment transport and deposition: A new implicit and O(N) method for inverse analysis. *Earth and Planetary Science Letters*, 524, 115728.

Zachos, J., Pagani, M., Sloan, L., Thomas, E., and Billups, K. (2001). Trends, rhythms, and aberrations in global climate 65 Ma to present. *Science (New York, N.Y.)*, 292(5517), 686–693.

FIGURES CAPTIONS

Figure 1: Diffusion coefficients (K_d) values (in km^2/kyr) published and measured in this study.

Figure 2: Workflow of the estimation of the diffusion coefficient K_d . (a) Digitization of stratigraphic surfaces subdivided into segments bounded by pseudo-sections $X_{(i)}$. $Y_{S(i)}$ is the Two-way Travel Time (TWT in seconds) at each pseudo section intersection $X_{(i)}$ is the distance between two pseudo sections (horizontal sampling distance, ΔX). (b) Time to depth conversion. $Y'_{S(i)}$ is the depth (in meters) of intersection points. (c) Sand/clay ratio gradient along the sediment layer extrapolating lithologies $L_{W(i)}$ between wells $X_{W(i)}$. (d) Correction from post-depositional compaction. (e) Calculation of depositional rate $Q_{d(i)}$ and slope $S_{(i)}$ between pseudo-sections. (f) Estimation of diffusion coefficient K_d in environmental domains. K_d are the coefficient of the linear relation between deposition rates $Q_{d(i)}$ and slopes $S_{(i)}$.

Figure 3: Calculation of deposition rates (Q_d) from the ratio between the total amount of sediment which transited through the center point of each segment (A_T) and the time interval duration (ΔT). $A(i)$ is the area of sediment in the depositional domain (i) (proxy of the volume of sediments). $S(i)$ is the slope of the depositional domain (i).

Figure 4: (a) Range of the parameters values used to estimate accumulation rates (Q_d) and to restore slope (S) at time of deposition and the associated uncertainties. Calculations are repeated twenty time varying these parameters, within the indicated range, using a normal law. We then use the mean value of these twenty calculations to estimate K_d . (b) Example of uncertainties on the accumulation rates and the slopes for a given stratigraphic layer.

Figure 5: Location maps of the case studies (a) Ogooué delta and (b) Zambezi delta and their datasets (seismic lines, wells, reference sections). OCB: Ocean-Continent Boundary.

Figure 6: High-resolution seismic stratigraphy interpretations (a2, b2) and age models (a1, a3, b1, b3) of the Cenozoic Ogooué (a) and Zambezi (b) deltas. High resolution age models (a3, b3) established using the approach of Ponte et al. (2019).

Figure 7: Definition of depositional domains from paleobathymetries and slopes at time of deposition. (a) Example of the bathymetric profile (and associated slopes) of a stratigraphic surface. The bathymetry is estimated after restoration of the surface geometry at time of deposition using the backstripping method. (b) Box and Whisker diagrams of bathymetries for the different depositional domains for all the stratigraphic layers after restoration. (c) Box and whisker diagrams of slopes for each depositional domain of all restored stratigraphic surfaces.

Figure 8: Relationships between deposition rates (Q_d) and slopes (S) for two stratigraphic layers in the Ogooué delta for various time interval resolutions (ΔT) and distances of sampling (Δx). Dots are the mean value of twenty calculations including uncertainties related to time-depth conversion, sand/shale ratios, porosity corrections and calibrations in absolute ages.

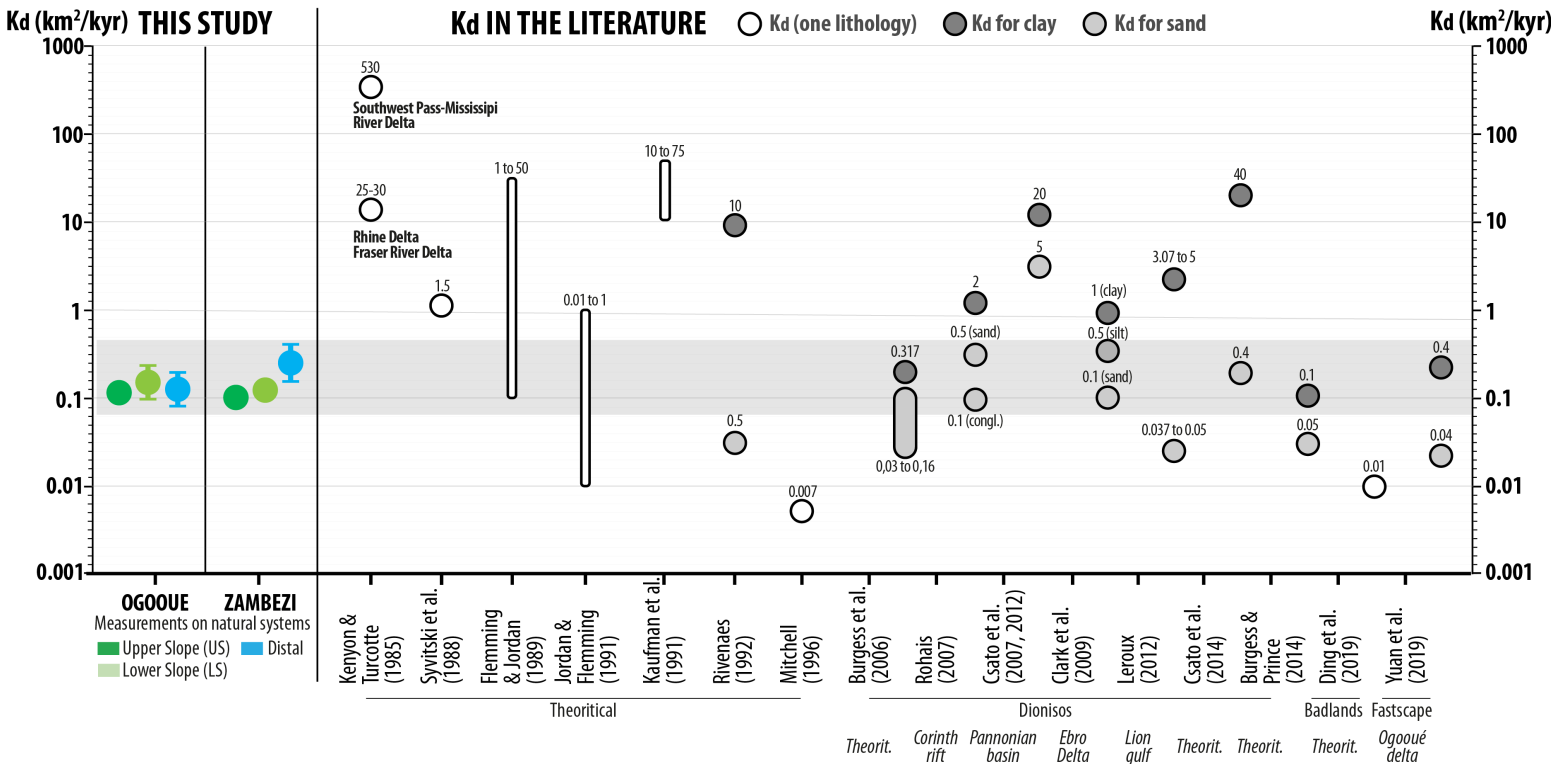
Figure 9: Diffusion/transport coefficient values for the Ogooué and Zambezi deltas at both low and high time (ΔT) and space (Δx) resolutions. (a) Box and whisker diagrams of all mean values (K_d) and coefficients of determination (R^2) for high (a1, a2) and low (a3, a4) resolutions in each depositional domain. (b) Box and whisker diagrams of mean values of K_d and coefficients of determination (R^2) at high (b1, b2) and low (b3, b4) resolutions for various bathymetries.

Figure 10: Box and whisker diagrams of mean high-resolution values of diffusion coefficients (K_d) for the Ogooué (a) and Zambezi (b) delta according to the stratigraphic context (Lowstand

Normal Regressive, LNR; Highstand Normal regressive, LNR and Transgressive T). For each system-track, K_d values are displayed according to different depositional domains.

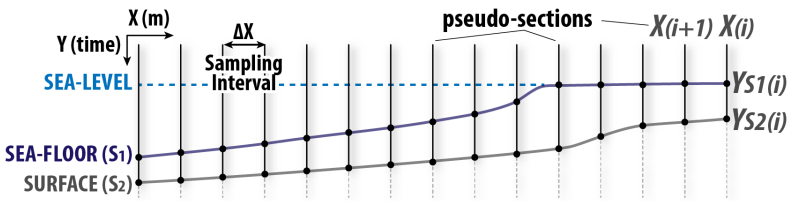
Figure 11: Evolution through time of slopes at time of deposition, depositional rates Q_d , diffusion coefficients K_d for the reference sections of the Ogooué (a) and Zambezi (b) deltas at both low and high resolutions. Eustasy (Miller et al., 2005) and surface-air temperature (De Boer et al., 2010) are shown in blue and green respectively.

Figure 12: Synthesis of measured K_d values and their variability along the depositional profile. Z.: Zambezi delta; O.: Ogooué delta.

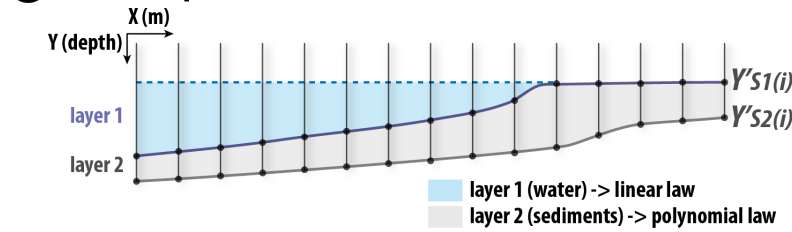


BRE_12696_Fig1.png

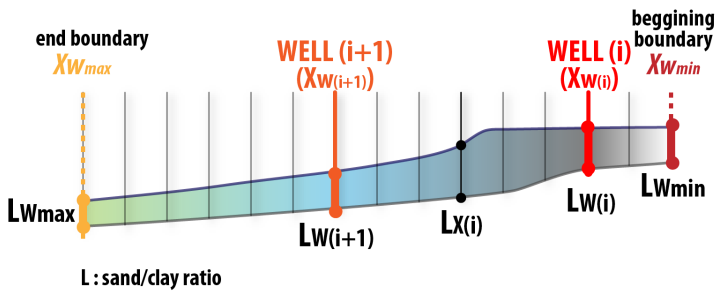
a digitization of stratigraphic surfaces



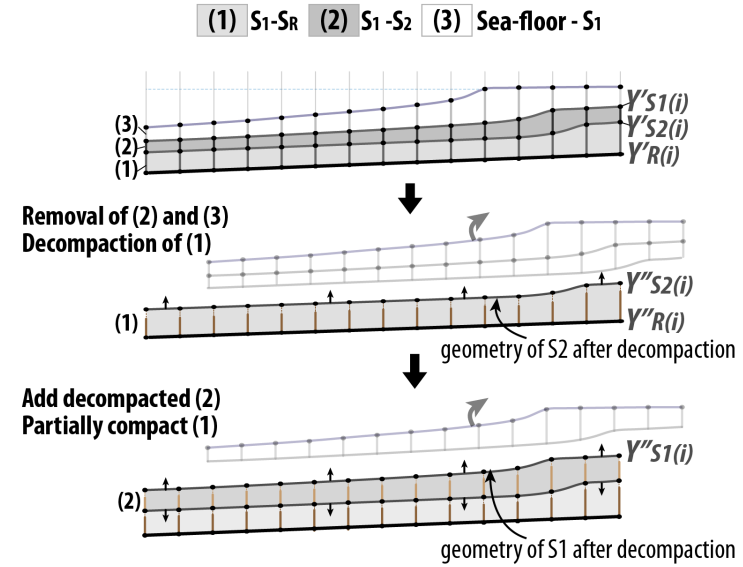
b time to depth conversion



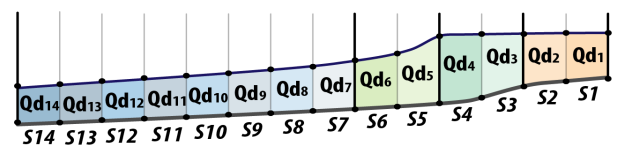
c lithological gradient



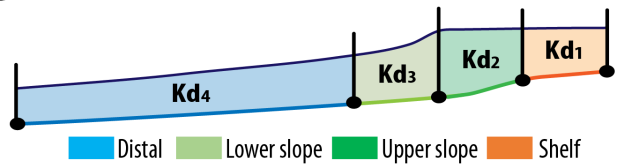
d differential decompaction



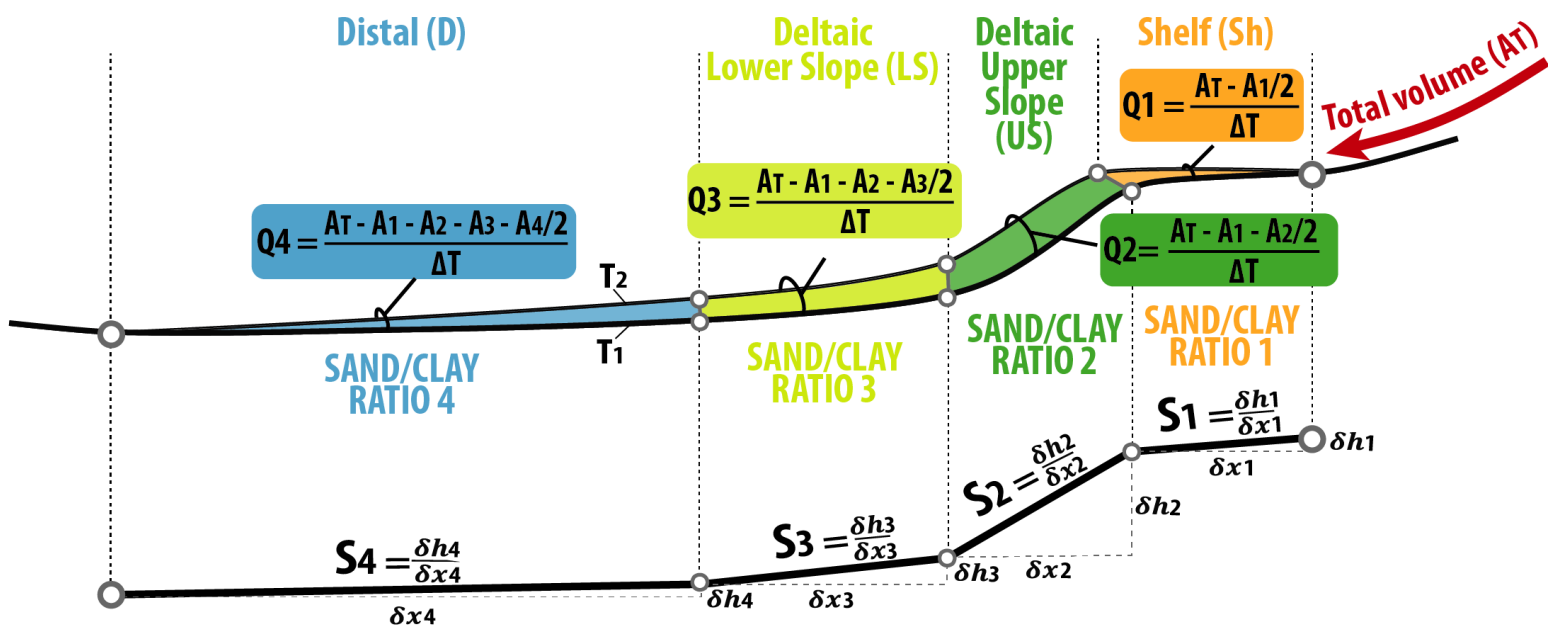
e calculation of depositional rates (Qd) and slopes (S)



f Estimation of diffusion coefficient (Kd)



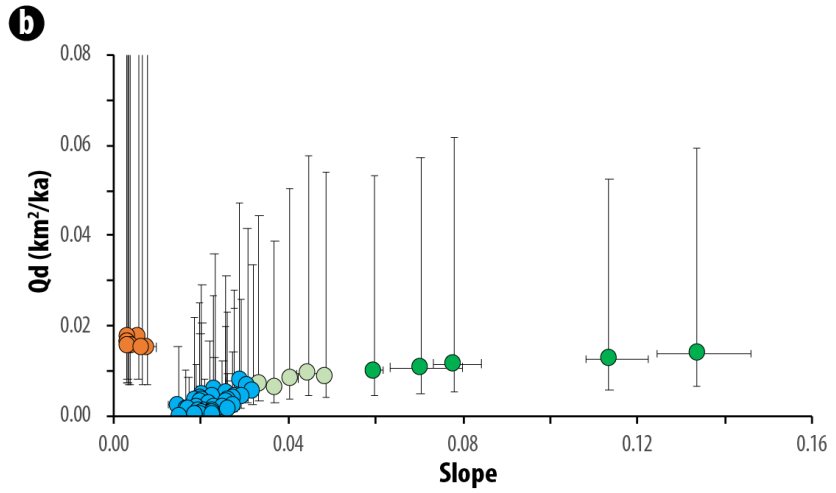
BRE_12696_Fig2.png



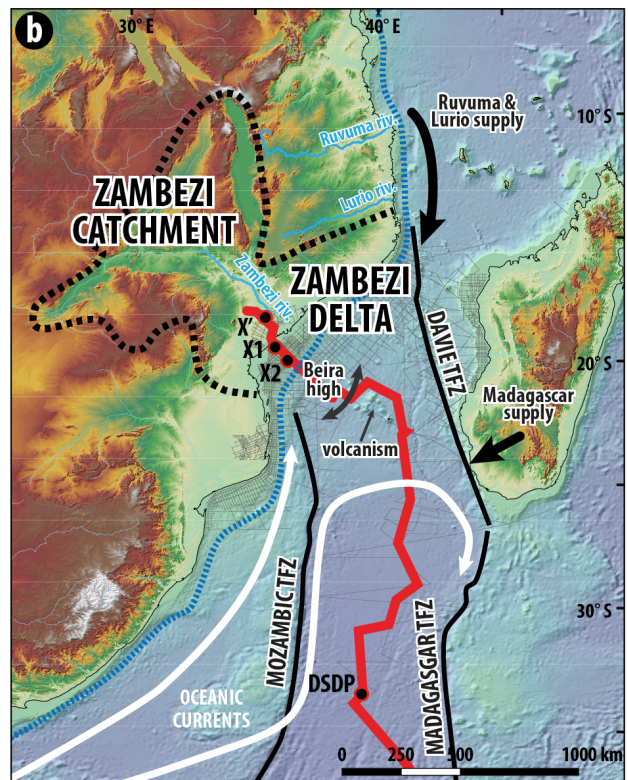
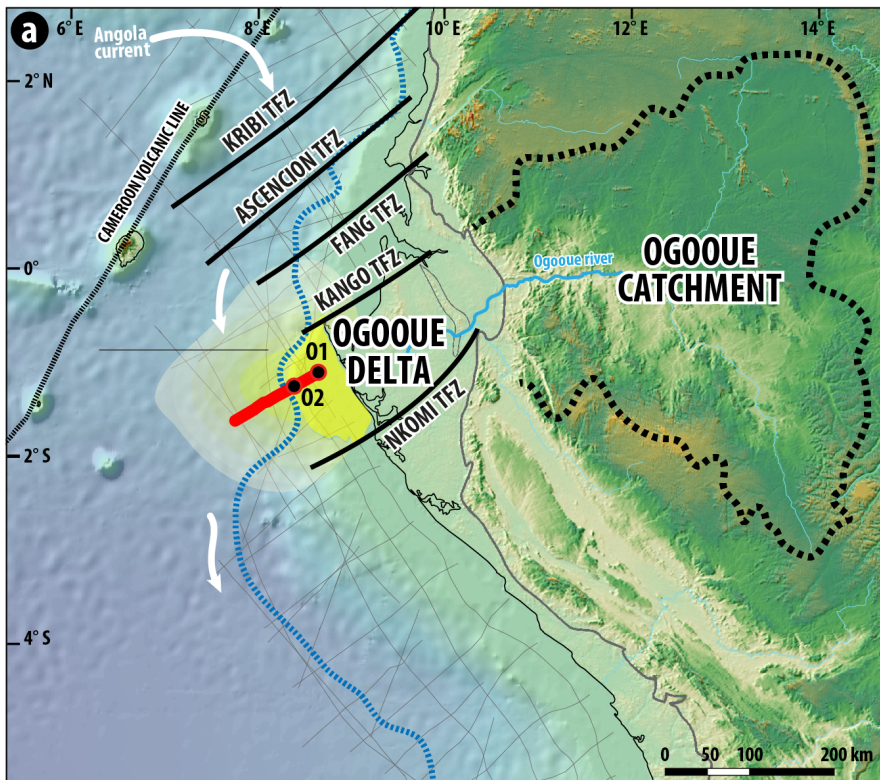
BRE_12696_Fig3.png

a

Sand/clay ratio	+/- 20 %	
Time/depth conversion	a : +/- 0.05 with a & b coefficient of b : +/- 0.1 2nd order polynomial law	
Coeff. compaction C Surface porosity Φ_0	<i>Sand</i>	Φ_0 min : 0.39 C min : 0.246
		Φ_0 max : 0.49 C max : 0.52
	<i>Shale</i>	Φ_0 min : 0.26 C min : 0.312
		Φ_0 max : 0.64 C max : 0.796
	Φ_0 in %	C in km^{-1}
Time interval	<i>Ogooue</i> +/- 0.1 Ma (LR) +/- 0.02 to 0.1 (HR)	<i>Zambezi</i> +/- 0.2 to 0.5 Ma (LR) +/- 0.05 to 0.2 Ma (HR)

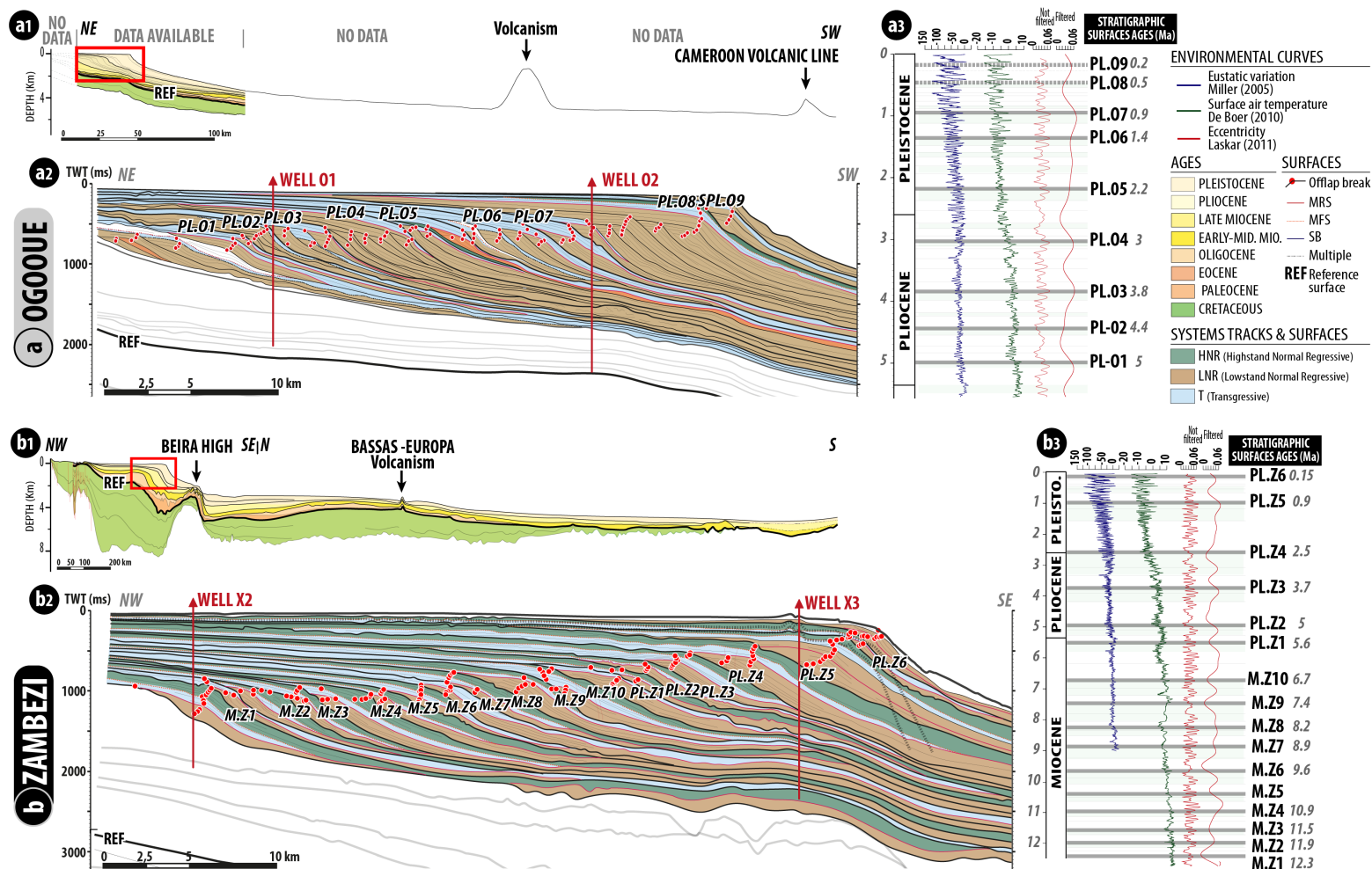


BRE_12696_Fig4.png



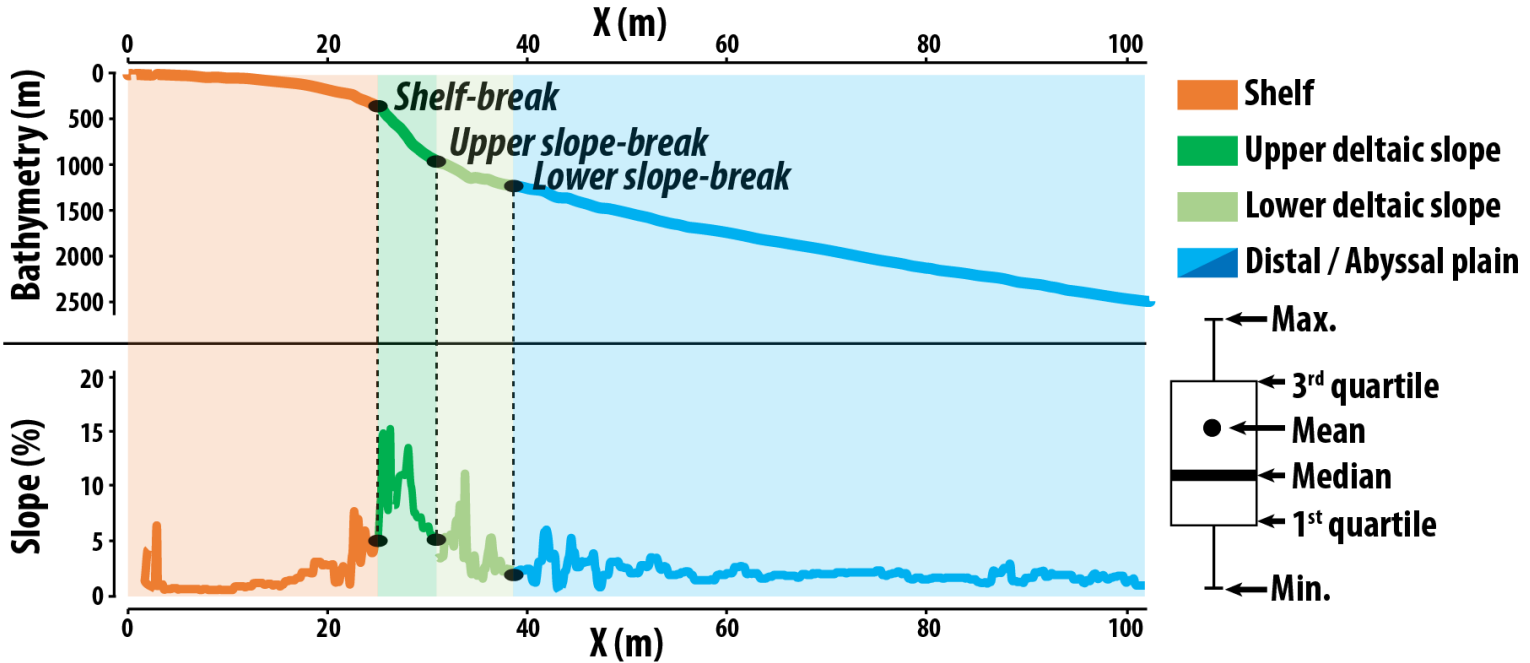
— Reference section
 ⋯ OCB
 — Seismic line
 — Fracture Zone
 ⋯ Catchment
 ● Well
 → Oceanic current

BRE_12696_Fig5.png

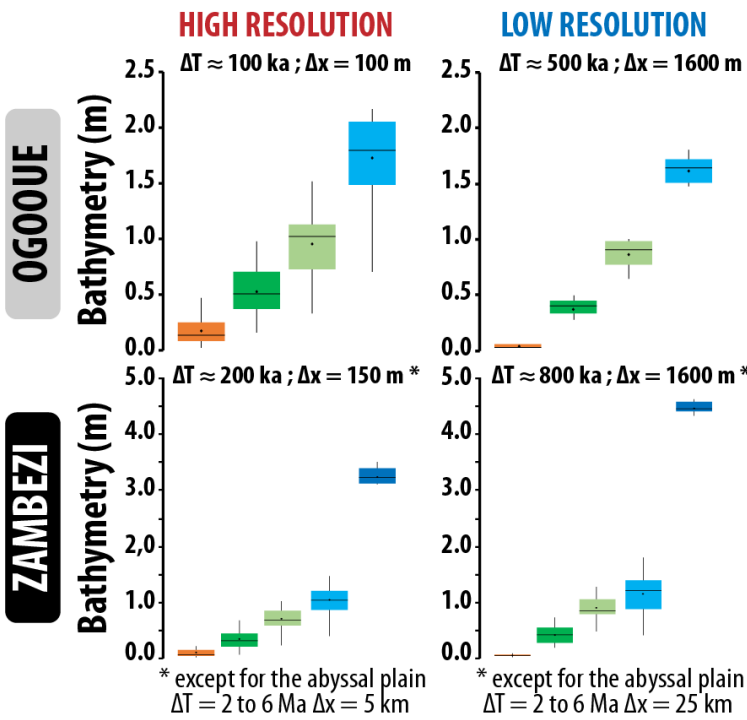


BRE_12696_Fig6.png

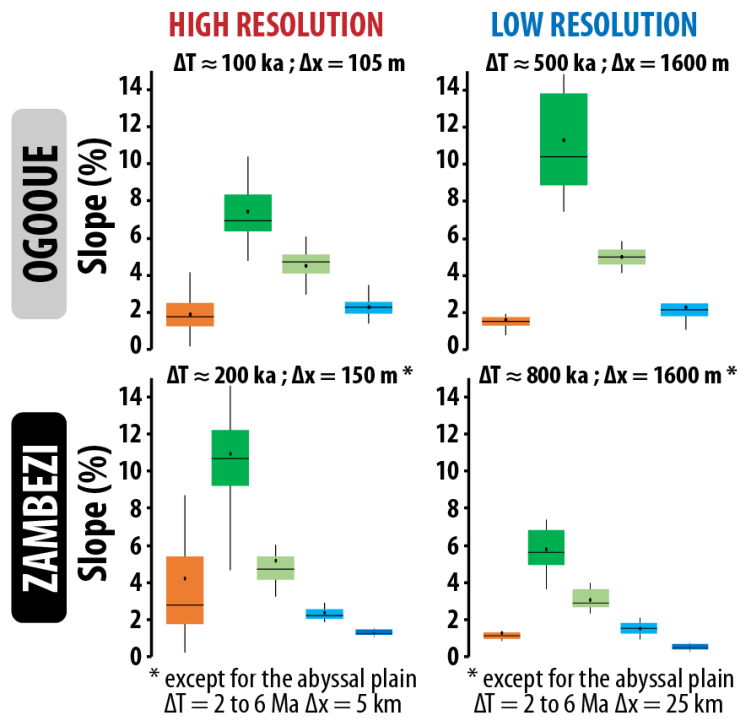
a DEFINITION OF DEPOSITIONAL DOMAINS FROM BATHYMETRY AND SLOPE



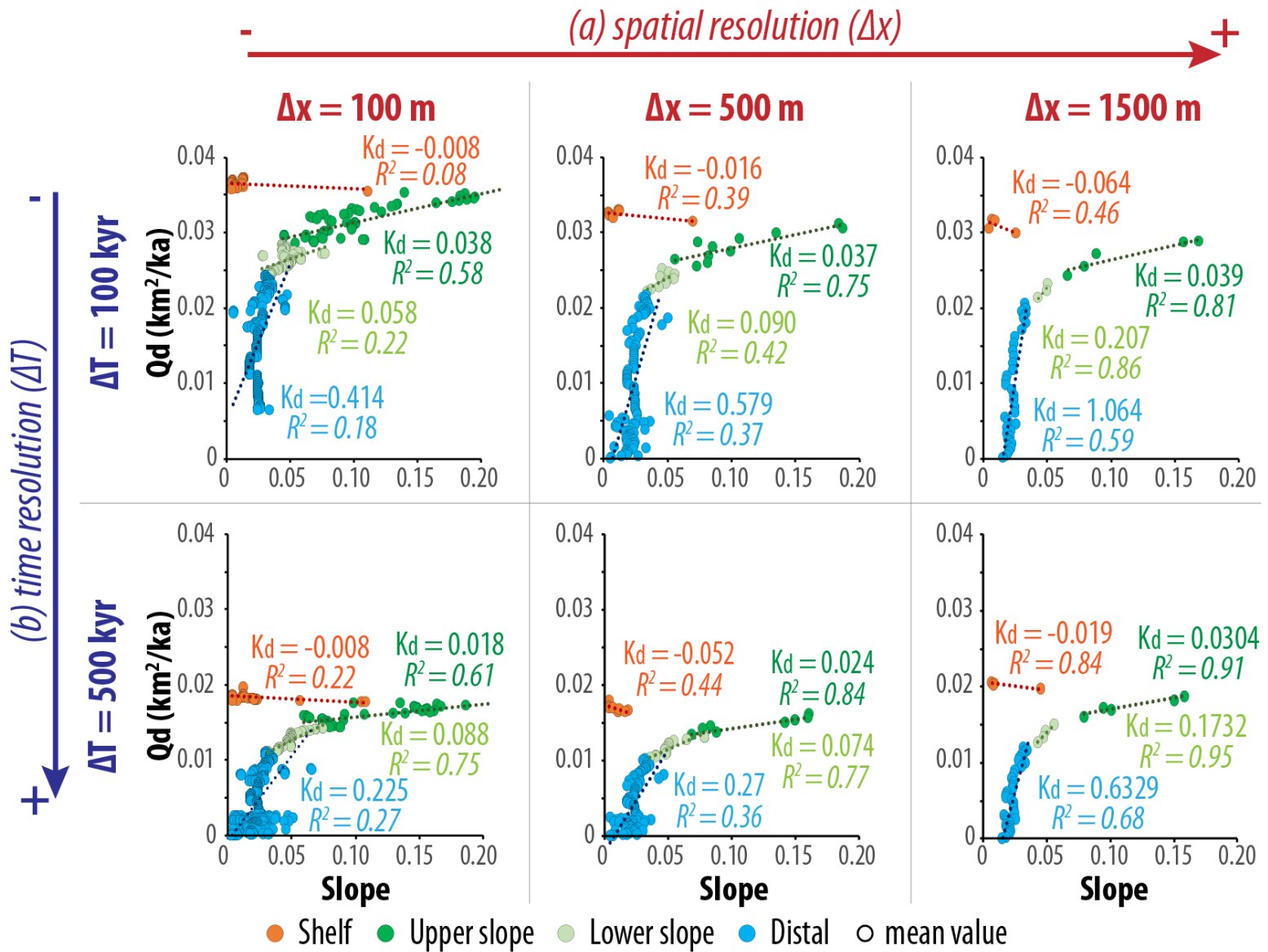
b DEPOSITIONAL DOMAINS BATHYMETRIES



c DEPOSITIONAL DOMAINS SLOPES

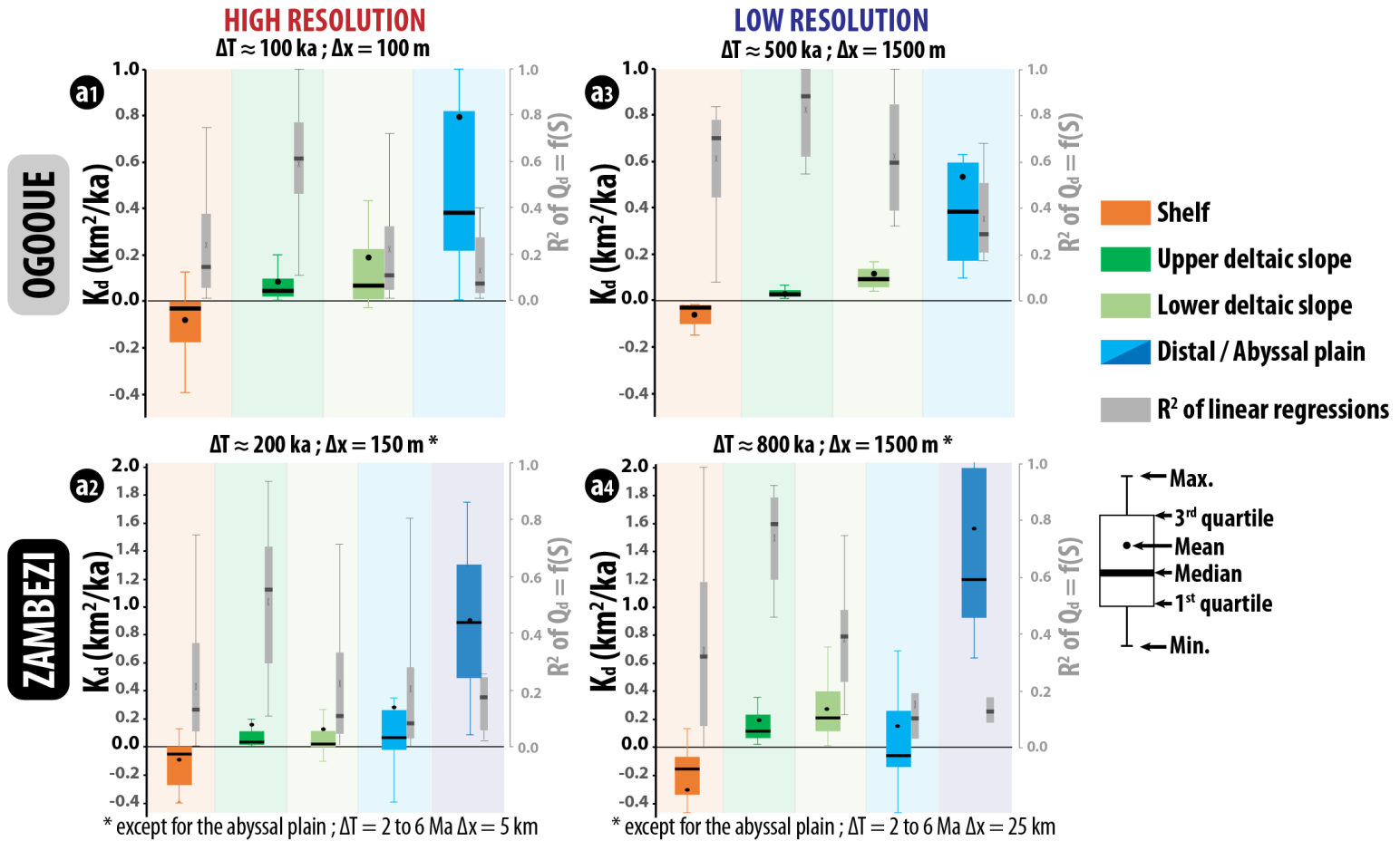


BRE_12696_Fig7.png

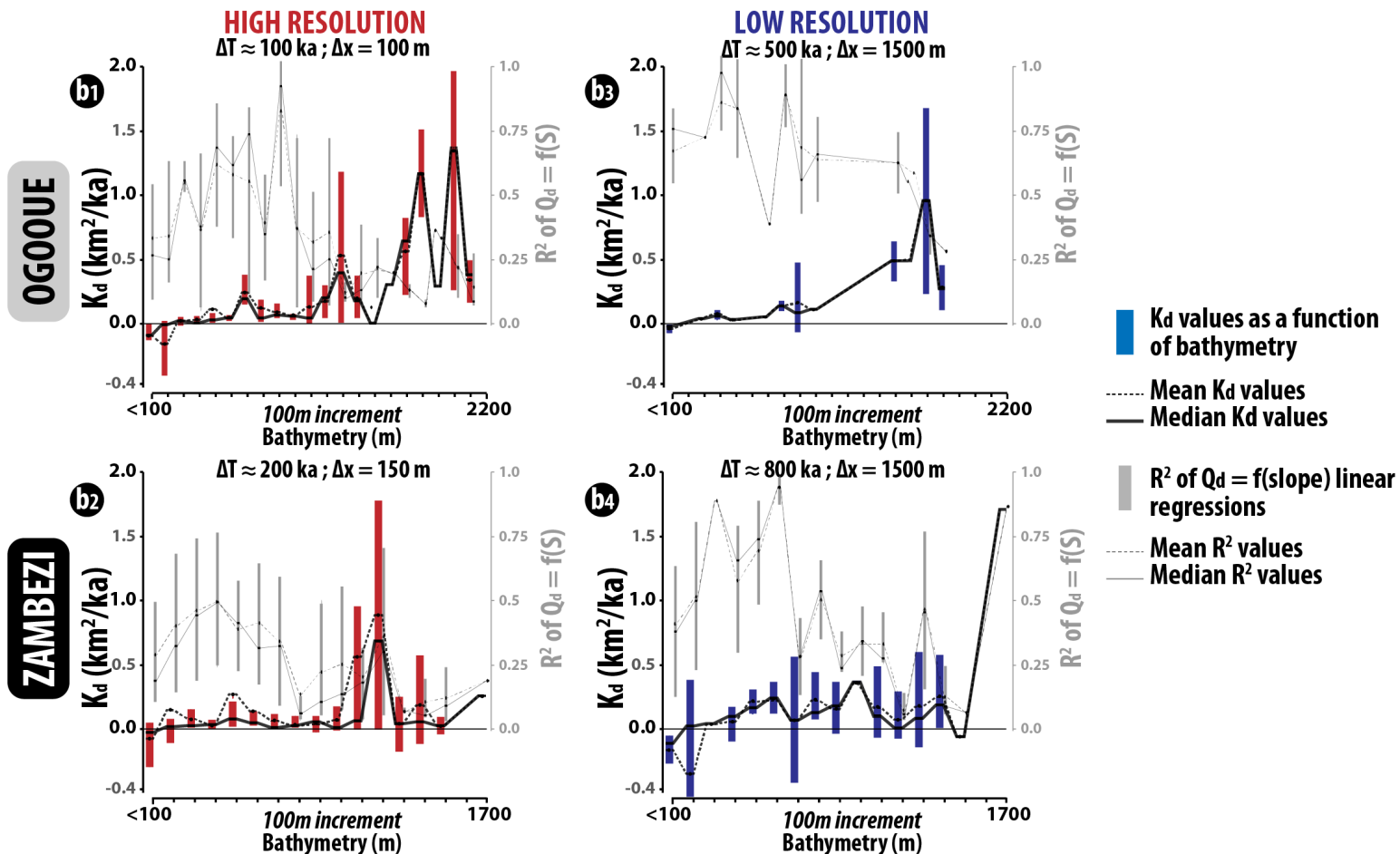


BRE_12696_Fig8.png

a Values of diffusion coefficient (K_d) according to depositional domains

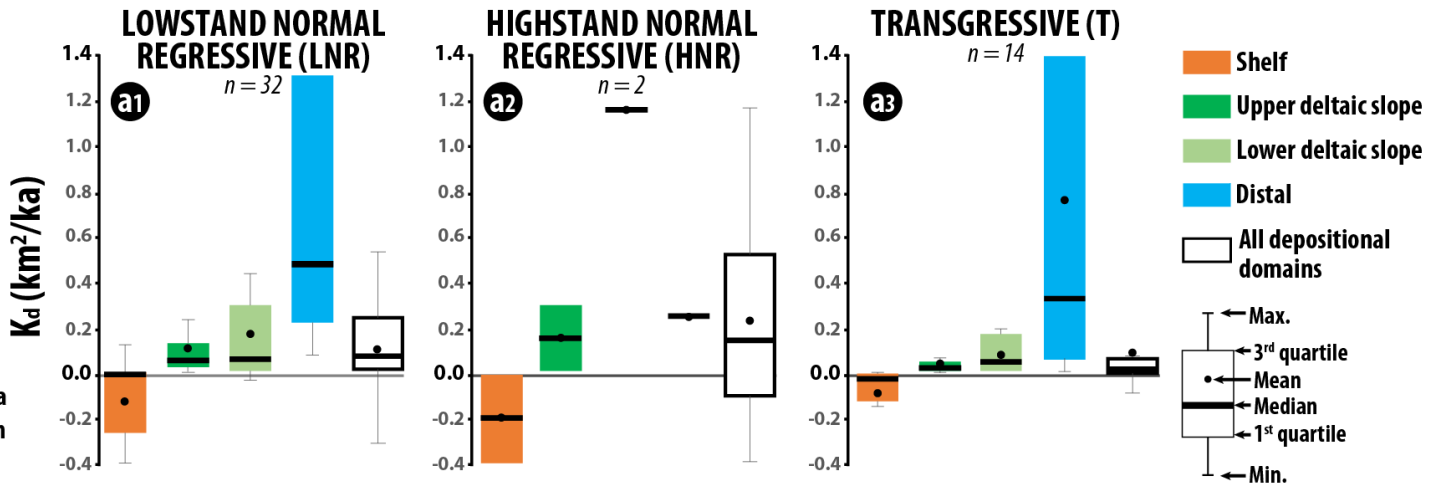


b Values of diffusion coefficient (K_d) according to bathymetries



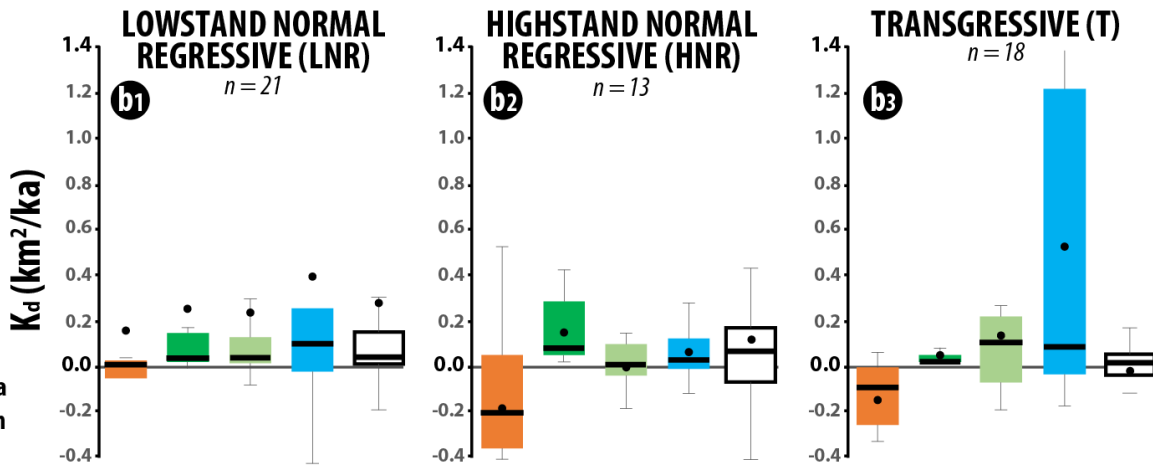
OGOOUE

$\Delta T \approx 100$ ka
 $\Delta x = 100$ m

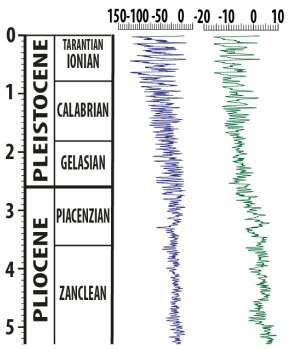
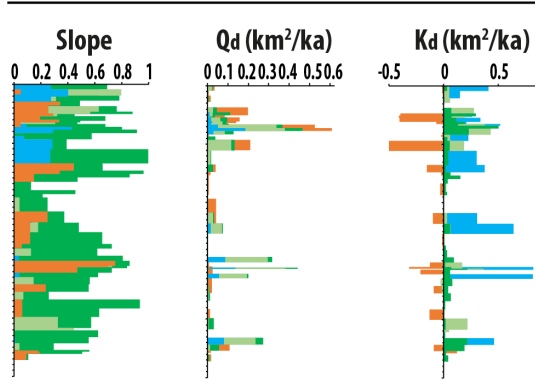
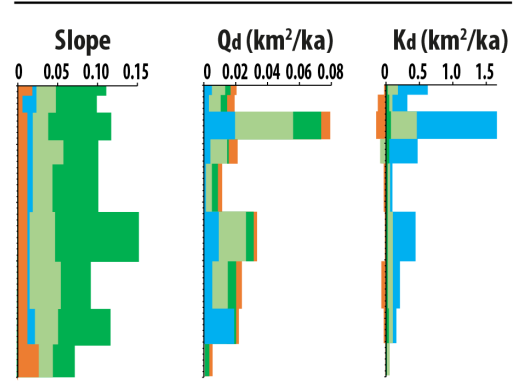
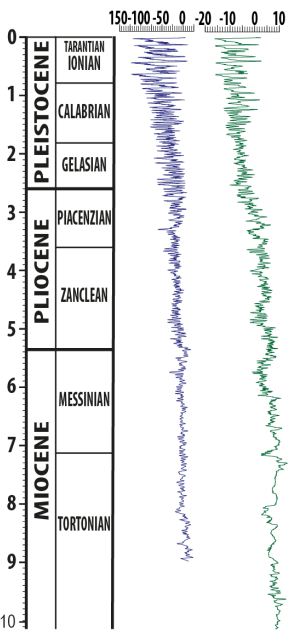
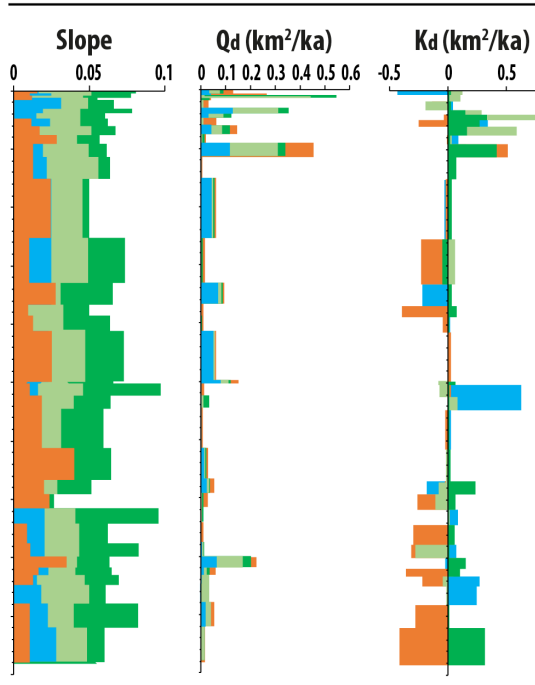
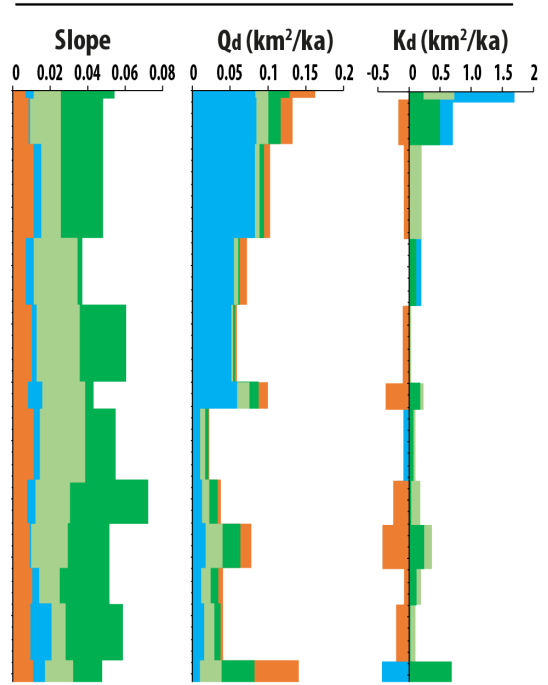


ZAMBEZI

$\Delta T \approx 200$ ka
 $\Delta x = 150$ m



BRE_12696_Fig10.png

aEustatic Surface
variation air temp.**OGOOUÉ****HIGH RESOLUTION**
 $\Delta T \approx 100 \text{ ka}$; $\Delta x = 100 \text{ m}$ **LOW RESOLUTION**
 $\Delta T \approx 500 \text{ ka}$; $\Delta x = 1500 \text{ m}$ **b**Eustatic Surface
variation air temp.**ZAMBEZI****HIGH RESOLUTION**
 $\Delta T \approx 200 \text{ ka}$; $\Delta x = 150 \text{ m}$ **LOW RESOLUTION**
 $\Delta T \approx 800 \text{ ka}$; $\Delta x = 1500 \text{ m}$ 

■ Shelf
 ■ Upper deltaic slope
 ■ Lower deltaic slope
 ■ Distal

BRE_12696_Fig11.png

